FATIGUE PERFORMANCE OF VARIABLE MESSAGE SIGN & LUMINAIRE SUPPORT STRUCTURES
Volume II – Fatigue Testing and Failure Analysis of Aluminum Luminaire Support Structures

FINAL REPORT
May 1998

Submitted by

Gary R. Consolazio*
Professor

Kevin W. Johns**
Graduate Research Assistant

Robert J. Dexter ***
Associate Professor

* Center for Advanced Infrastructure and Technology
Civil & Environmental Engineering
Rutgers, The State University
Piscataway, NJ 08854-8014

** Lehigh University
ATLSS Engineering Research Center
117 ATLSS Dr., Imbt Laboratories
Bethlehem, PA 18015-4729

*** Dept. of Civil Engineering
University of Minnesota

NJDOT Research Project Manager
Mr. Nicholas Vitillo

Disclaimer Statement

1. Report No. FHWA 1998 – 010	2. Government Accession No.	3. Recipient's Catalog No.
4. Title and Subtitle Fatigue Performance Of Variable Message Sign & Luminaire Support Structures Volume II – Fatigue Testing and Failure Analysis of Aluminum Luminaire Support Structures		5. Report Date May 1998
		6. Performing Organization Code CAIT/Rutgers/ATLSS/Lehigh
7. Author(s) Gary R. Consolazio, Kevin W. Johns, and Robert J. Dexter		8. Performing Organization Report No. FHWA 1998 - 010
9. Performing Organization Name and Address New Jersey Department of Transportation CN 600 Trenton, NJ 08625		10. Work Unit No.
		11. Contract or Grant No.
12. Sponsoring Agency Name and Address Federal Highway Administration U.S. Department of Transportation Washington. D.C.		13. Type of Report and Period Covered Final Report 09/13/1996 - 6/30/1998
		14. Sponsoring Agency Code

15. Supplementary Notes

16. Abstract

In Order to determine equivalent static pressures for fatigue loads on cantilevered highway support structures a cantilevered Variable Message Sign(VMS) located along Interstate westbound at mile marker 48.5 in northern New Jersey was continuously monitored for three months. The structure was instrumented with strain gages, pressure transducers, and a wind sentry. All the data was collected with a Campbell Scientific CR9000 digital data acquisition system. A cellular phone transceiver enabled remote communication with the data logger. The system and instrumentation was powered with solar powers and marine batteries. Short-term testing was performed on the structure to determine the dynamic characteristics such as stiffness, natural frequency, and percent of critical damping. Results of the short-term test indicated that the stiffness was 0.24 kN/mm, the first and the second modes were 0.87 cycles/s and 1.22 cycles/s respectively, and the percent of critical damping for the first and second modes were 0.57 percent and 0.25 percent respectively. Long-Term monitoring was performed to capture the structures response to natural wind gusts, galloping, and truck-induced wind gusts. This data would then be used to determine appropriate fatigue design wind loads for future sign support structures. During the three months of monitoring the structure did not experience galloping, which is a phenomena highly dependent on location. A galloping design pressure of 1000 Pa was recommended based on previous research. The summer months, which is when the structure was monitored, were not conductive to the strongest natural winds patterns in Northern New Jersey. The highest natural wind speed that was recorded was 7.5m/s. It is believed that much stronger winds are present in winter and spring, therefore a natural wind gust design pressure of 250 Pa was recommended. Truck-induced gusts were measured and a linear gradient for the truck-induced gust design pressure was determined. The truck-induced gust design pressure ranged linearly from 1760 Pa at 0 to 6m above the surface of the road to 0 Pa at 10.1m and over.

17. Key Words fatigue, failure analysis, loads, highway, support structures, cantilever, VMS	18. Distribution Statement

19. Security Classif (of this report) Unclassified	20. Security Classif. (of this page) Unclassified	21. No of Pages 76	22. Price

Form DOT F 1700.7 (8-69)

FATIGUE TESTING AND FAILURE ANALYSIS OF ALUMINUM LUMINAIRE SUPPORT STRUCTURES

Final Report

by

Kevin W. Johns
Graduate Research Assistant
Lehigh University

Robert J. Dexter
Associate Professor of Civil Engineering
University of Minnesota

**ATLSS is a National Center for Engineering Research
on Advanced Technology for Large Structural Systems**

117 ATLSS Drive
Bethlehem, PA 18015-4729

Phone: (610)758-3535	www.lehigh.edu/~inatl/inatl.html
Fax: (610)758-5553	Email: inatl@lehigh.edu

Acknowledgments

Table of Contents

List of Tables

List of Figures

Chapter 1 - Introduction

1.1 Problem

Luminaires are used at various locations on major highways and in towns for the purpose of roadway illumination. Luminaire supports come in a variety of configurations and materials. The two most common configurations are a single support with a cantilevered arm and a single, straight support with the light directly on top. Luminaire supports are made from aluminum and from galvanized steel. The cantilevered aluminum luminaire supports that were being researched have the designation of L-8-S-40SB by the New Jersey Department of Transportation (NJDOT) and have a configuration as shown in (Figure 1-1). The straight aluminum luminaire supports that were being researched have the designation of L-E-S-45 by NJDOT and have a configuration as shown in Figure 1-2. These support structures were all manufactured by Hapco and installed by NJDOT.

Recently there were 8 straight and 6 cantilevered luminaire supports that failed along Route 147 in New Jersey. The cantilevered luminaire supports were mounted directly to the parapet of the Grassy Sound Bridge, which is part of Route 147. These cantilevered supports experienced cracking around the shoe base-to-pole weld (Figure 1-3) and at the welds around the hand access holes. The straight poles were used along the side of the road leading up to the bridge. These straight poles were connected to their foundation through the break-away transformer base. All of the poles that were on a transformer base experienced failure through the transformer base (Figure 1-4) and not in the pole or shoe base.

Many other states have reported large amplitude vibrations in their luminaire support standards and in some instances the structures fail. The large amplitude vibration is made possible by the combination of low stiffness and low critical damping ratio in the support structures. These structures have been known to vibrate in both first and second modes. The second mode vibration is believed to be caused by vortex shedding.

The effects of vortex shedding on luminaires were recently studied at the Advanced Technology for Large Structural Systems Engineering Research Center (ATLSS) at Lehigh University for the National Cooperative Highway Research Program (NCHRP). The project was NCHRP 10-38, "Fatigue-Resistance Design of Cantilevered Signal, Sign and Light Supports", which dealt with determining what types of structures would be effected by wind phenomena such as vortex shedding and determining appropriate design fatigue loads for these structures [1].

1

1.2 Purpose

The primary purpose of the research described in this report was to determine the fatigue resistance of the socket detail used on the NJDOT luminaire standards and determine what caused the failure of multiple luminaire supports on Route 147 in southern New Jersey. To accomplish this objective 12 luminaire support standards were sent to ATLSS to determine the fatigue resistance of the socket joint at the pole to shoe base connection. Pull tests were also performed to determine the dynamic characteristics, such as stiffness, natural frequency and percent of critical damping of each type of luminaire standard.

1.3 Scope

This report summarizes previous research relevant to the fatigue strength of the socket detail in question. A concrete base was cast to replicate actual foundation conditions of a luminaire standard installed in the field. This base was then used in the fatigue tests and the pull tests. The fatigue testing enabled a decision to be made on the appropriate fatigue strength of the socket connection. Finite element analysis was used to calculate the dynamic characteristics of the luminaire standards. These analytical values were then compared to the measured dynamic characteristics observed during the pull tests.

In addition to this research on the fatigue strength of these poles, a failure analysis was conducted on pieces of the failed poles. The report on this failure analysis was presented previously [15].

This research was not concerned with determining appropriate mitigation devises for the vibration problems. Mitigation is to be addressed in the phase two studies of NCHRP project 10-38, which are ongoing at the University of Minnesota under the direction of Robert Dexter.

8'-0" OR 15'-0" (BRACKET ARM)

SEE NOTE #1

3" RISE

LUMINAIRE AS SPECIFIED

CAP CAST ALUM. ALLOY

ALUM. ALLOY 6061-T6. OR 6063-T6. ⅜ PLATE

ALUM. OR PLASTIC END CAP

7 ½" STRAIGHT END OF ARM - 2 ⅜" O.D.

6063-T6 ALUM. ALLOY .125 MIN. THK. WALL

1 ½"X ⅜" ELLIPTICAL EXTRUDED STRUT ALUM. ALLOY 6061-T6 OR 1 ¼" SCH. 40 PIPE ALUM. ALLOY 6063-T6

DRILL FOR 1" I.D. RUBBER GROMMET POLE SUPPLIER SHALL FURNISH 1" I.D. RUBBER GROMMET

ALUMINUM SPLIT CAST OR EXTRUDED CLAMPS. DESIGN SHALL BE SUBMITTED FOR APPROVAL. STAINLESS STEEL HARDWARE SHALL BE SUPPLIED. SEE NOTE #3.

DIMENSIONS FOR VARIOUS TYPES SHOWN ON SCHEDULE - I

6063-T6 ALUM.ALLOY SATIN GROUND FINISH 8"Ø TO 6"Ø TAPER SHAFT

3'-0"

6"DIA. STRAIGHT SHAFT

LIMIT OF TAPER

REINFORCED HANDHOLE SEE NOTE #6 GROUND STUD OPPOSITE HANDHOLE

SHOE BASE SEE NOTES #3 & #4 AND #13

TOP OF BASE 13 ½" SQ.

11" TO 12" DIA. BOLT CIRCLE

TRANSFORMER BASE SEE DETAIL L-21

⅜" MIN. BASE THK.

17"

Figure 1-1 Cantilevered Luminaire Support Structure

SEE ADAPTER DETAIL

TAPERED ALUM. ALLOY TUBE 6063-T6
SATIN GROUND FINISH

LIMIT OF TAPER

INTERNAL VIBRATION DAMPER TO
BE INSTALLED PER MANUFACTURER
SPECIFICATION

⅝" DIA. STN. STL. THRU BOLT, HEX NUT,
& LOCK WASHER (FIELD DRILL @ ASSY.)

ALUM. ALLOY TUBE 6063-T6
SATIN GROUND FINISH

SHOE BASE

11" TO 12" BOLT CIRCLE

TRANSFORMER BASE.
FOR DETAILS SEE DRAWING L-21

3'-0"
6" DIA. STRAIGHT SHAFT

18'-0"

15' TAPER
TAPER

1'-0"
MIN.
6"

42'-0"
SHAFT

24'-0"

17"

Figure 1-2 Straight Luminaire Support Structure.

4

LOCATION OF CABLE OUTLET
AS SHOWN ON POLE SHAFT IN
RELATION TO SHOE BASE

$2\frac{1}{2}$"RAD. MAX.
SEE NOTE #3

$\frac{5}{16}$"

D   40°   D

$5\frac{1}{2}$" R

6" R

$11\frac{1}{4}$"-12"

11"DIA. BOLT CIRCLE

12"DIA. BOLT CIRCLE

$11\frac{1}{4}$"-12"

ALUMINUM ALLOY 356-T6 ASTM SPEC. NO. SAND
CST'G B26 OR PERM. MOLD CST'G B108
ASTM ALLOY DESIG. SG 70A

CONTINUOUS WELD
INERT GAS METHOD

$8\frac{7}{8}$"

$\frac{1}{16}$"

TO BE MACHINED BEFORE
ASSEMBLING TO RECEIVE
BASE END OF SHAFT
$\frac{1}{2}$"

$\frac{1}{4}$"R

$\frac{3}{4}$"

ALUMINUM BOLT COVER
4 REQ'D. EACH SHAFT
1" R

$3\frac{1}{2}$" MIN.

$\frac{3}{4}$" MIN.

CONTINUOUS WELD
INERT GAS METHOD

$\frac{1}{8}$"R

$\frac{1}{8}$"

$\frac{5}{16}$"

$\frac{1}{8}$"

8.430" MAX.

45°

Figure 1-3 Shoe Base to Pole Connection.

5

TOP VIEW
N.T.S.

12" DIA. B.C.
11" DIA. B.C.
.45"

13⅛"
9¼"
11¾" MIN.
17"
8"
9¾"
13¾" MIN. - 14½" MAX.
15⅜"

A 4" LETTER
BE STENCILEI
ON THE OUTS
OPPOSITE THI

GROUND STUI
SEE DETAIL

.15" THICK NOI

ACCESS DOOF
TYPE ABS PL
STEEL GRAY
⅛" MINIMUM
SEE NOTE 1

ELEVATION
N.T.S.

15" DIA. BOLT CIRCLE
1⅜" TYP.
SEE NOTE 5

PLAN VIEW OF BASE
N.T.S.

Figure 1-4 Transformer Base.

6

Chapter 2 - Background

2.1 Wind Loading Phenomena Relevant to Luminaires

Luminaire supports are susceptible to two wind phenomena, natural wind gusts and vortex shedding. All structures are susceptible to natural wind gusts. Vortex shedding is a problem for luminaire supports because their shape enables the formation of uniform vortices to form around the structure.

2.1.1 Natural Wind Gusts

The response of typical cantilevered support structures to natural wind gusts was modeled using spectral finite-element analysis. The structure is broken up into several continuous areas such as signs or exposed portions of the structure. The fluctuating wind force on each area and the resulting response variables (such as column base moment) during a short interval are characterized as stationary random processes. The response spectrum can be related back to the expected variable-amplitude history of the response as a function of time. Specifically, the root-mean-square (RMS) of the random response time history is found from the integration of the response spectrum over all significant frequencies. In the case of luminaire support structures, there are only a few significant frequencies, therefore the integration is performed by simply summing the response at these frequencies.

The wind force spectrum is derived from the velocity spectrum. A standard wind velocity spectrum (which depends on the mean hourly wind velocity) was selected from the literature [2]:

$$S_V(f) = \frac{4KV_{10}^2 x^2}{f(1+x^2)^{4/3}} \qquad (2\text{-}1)$$

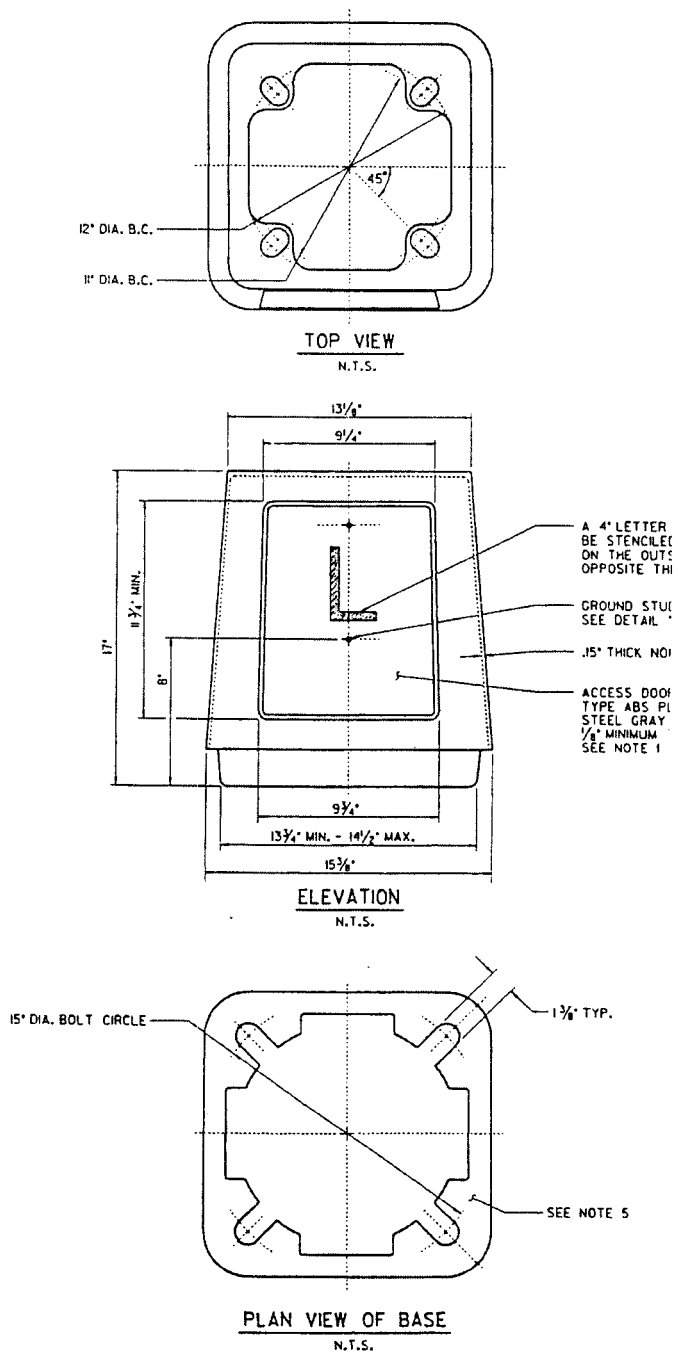where $S_V(f)$ is the spectral density of the velocity (which has units of velocity squared multiplied by time), f is the cyclic frequency (cps), K is a terrain coefficient $(m/s)^2$, V_{10} is the mean wind velocity (m/s) at a reference height of 10 meters, and x is the quantity (1200 meters * f)/V_{10} (dimensionless for V_{10} in m/s). The terrain coefficient K was taken as 0.005 which is typical for open grassy terrain [2,3].

The drag force is proportional to the square of the velocity and both the force and the velocity can be represented as the sum of their mean and fluctuating components. Through algebraic manipulation of these relationships, the following relations can be obtained [3]:

$$(\frac{d}{v})^2 = \frac{4\ D^2}{V^2} = 4\ C^2\ A^2\ V^2 \qquad (2\text{-}2)$$

7

where d and D are the fluctuating and mean value of the drag force respectively, v and V are the fluctuating and mean value of the wind velocity respectively, A is the total frontal area of the surface which is causing the drag, and C is a constant equal to $0.5rC_d$ with r equal to the density of air and C_d equal to the drag force coefficient. The density was taken as 1.22 kg/m^3 which is the value for "standard air" (one atmosphere pressure at 14°C).

The force and velocity spectra are proportional to the square of the fluctuating components of force or velocity, velocity, therefore the ratio of these spectra is equal to the ratio in Equation 2-3, i.e.:

$$S_F(f) = 4 \ C^2 \ A^2 \ V^2 \ S_v(f) \qquad (2\text{-}3)$$

The force spectrum must be calculated for the total frontal area of a surface and cannot be broken down into sub-areas. One spectrum is calculated for each luminaire attachment. Additional spectra are calculated for each continuous exposed portion of the cantilevered arm or pole. These spectra must be completely correlated to each other in the analysis.

Important assumptions must be made regarding: 1) the mean wind velocity at which the support structures should be analyzed; and, 2) estimating the effective stress range from the RMS of the variable amplitude response. It is impractical to forecast the future wind history at each location for luminaire support structures. Therefore, some very simple assumptions were made. The design procedure is based on a spectral analysis using the mean hourly wind velocity, which was exceeded in only 0.01 percent of all hours. It is accepted that the probability of exceedence of mean hourly wind velocity at a location is a Rayleigh distribution, which depends only on the yearly mean wind velocity V_m[4], i.e.:

$$P_E(v) = e^{\frac{-\pi v^2}{4V_m^2}} \qquad (2\text{-}4)$$

where $P_E(v)$ is the probability that a randomly-occurring mean hourly velocity is greater than the velocity magnitude v and e is the base of the natural logarithms. The limit-state mean hourly velocity is found by setting P_E equal to 0.01 percent and solving for v.

The yearly mean wind velocity also varies from place to place. A collection of yearly mean wind speed data from weather stations at 59 cities across the U.S. was examined. Most weather stations are located at airports, therefore the data should be representative of most open terrain. The data showed that 81 percent of the cities had a mean wind velocity at 10 m (33 ft) above the ground less than 5 m/s (11 mph). It was decided to use 5 m/s (11 mph), which was exceeded in only 19 percent of U.S. cities, as the baseline case for a static design pressure in the specifications. The mean hourly wind velocity for this yearly mean wind speed is 17 m/s (37 mph).

The result of the analysis, the spectral density of the response, has units of the response (such as moment or stress) squared multiplied by time. When the spectral density of the response is integrated across a range of frequencies, the result (the area

8

under the spectrum) is equivalent to the variance of the response about the mean. The square-root of this area is the root-mean-square (RMS) of the response. The time history of the response is narrow-banded (concentrated about one frequency), since the response is still dominated by the resonant frequency. For random, narrow-band time histories, the average or effective stress range S_r^{eff} can be estimated from the relationship which gives the stress range for a constant-amplitude response in terms of the RMS of the stress response σ_{rms}[5], i.e.:

$$S_r^{eff} = 2.8\,\sigma_{rms} \tag{2-5}$$

A variety of sign, signal, and luminaire support structures were analyzed at a mean wind velocity of 17 m/s and values of normalized equivalent static pressures for these structures ranged from 170 to 300 Pa (3.6 to 6.3 psf). Considering the numerous uncertainties in this analysis, not enough is known to assign greater or lesser loads to different types of structures. Also, separate loading for different types of structures would unnecessarily complicate the design process. Therefore, these values were averaged and rounded to 250 Pa (5.2 psf), which is recommended for design. This natural wind gust pressure must be applied to a variety of surfaces with widely varying drag coefficients. Therefore the recommended static design pressure must be multiplied by the appropriate drag coefficient and then may be applied to the surface. The structures should be designed so that the stress ranges resulting from the application of this load range are below the constant amplitude fatigue limit (CAFL) [1].

These calculations indicate that most structures will eventually be susceptible to cracking from natural wind gusts, but the recommended loads are not so large as to predict rapid failure. These results are consistent with observed service fatigue failures that can be attributed to natural wind gusts. Because of the uncertainty in these assumptions, the recommended equivalent static load range can be easily adjusted for other mean wind speeds.

2.1.2 Vortex Shedding

Vortex shedding typically develops during steady, uniform flows, and produces resonant oscillations in a plane normal to the direction of flow. Vortex shedding is caused by the shedding of vortices in a regular, alternating pattern in the wake of a structural element. The phenomenon has been observed in a wide-range of structures, including chimneys, hyperbolic cooling towers, antenna masts, and pipelines.

When a structural element is exposed to a steady, uniform flow, vortices are shed in the wake behind the element in an alternating pattern commonly referred to as a Von Karman vortex street. The frequency at which vortices are shed from the element, f_s, is given by the Strouhal relation:

$$f_s = \frac{SV}{D} \tag{2-6}$$

9

where S is the Strouhal number, D is the across-wind dimension of the element, and V is the free-stream wind velocity. As is indicated by Equation 2-6, the frequency at which vortices are shed is dependent upon the velocity of the flow, the across-wind dimension of the element, and the shape of the element (as defined by the magnitude of the Strouhal number). The Strouhal number for a luminaire with a round cross section, or with the same geometry as the poles on Route 147, is 0.18.

When the frequency of vortex shedding, as predicted by the Strouhal relation, does not match one of the natural frequencies of the structure, the shedding of vortices in the wake of a structure will elicit only a nominal periodic response. However, when the frequency of vortex shedding approaches one of the natural frequencies of a flexible, lightly-damped structure, significant displacement ranges and stress ranges can result. The across-wind resonant vibration has a strong organizing effect on the pattern with which vortices are shed. The result is an increase in vortex strength, an increase in the spanwise correlation of the vortex shedding forces, and a tendency for the vortex shedding frequency to become coupled to the natural frequency of the structure. This phenomenon is called "lock-in". The critical wind velocity, V_{cr}, at which lock-in occurs is given by the Strouhal relation:

$$V_{cr} = \frac{f_n D}{S}$$

(2-7)

where f_n is the natural frequency of the structure. The result is a condition of resonant vibration that persists over a range of wind velocities.

The amplitudes of vibration associated with the lock-in phenomenon are generally limited by the ability of vortices to be shed from the structure in a symmetric pattern. Large amplitudes of vibration tend to interfere with the symmetric pattern of vortex formation. Previous research indicates that the maximum amplitudes of displacements associated with the lock-in phenomenon rarely exceed approximately 1 to 1.5 times the across-wind dimension of the structural element from which vortices are shed [6,7].

The fact that uniform steady-state flow is required for vortex shedding can be used to bound the velocities under which various elements of luminaire support standards could possibly be susceptible to vortex-induced vibrations. Previous research indicates that the level of turbulence associated with wind velocities above approximately 15 to 20 m/s (35 to 45 mph) limits the symmetric formation of periodic vortices [7]. Also, vortex formation at wind velocities below approximately 5 m/s (10 mph) generates forces with magnitudes insufficient to excite most structures. Based upon this knowledge, structures may be susceptible to vortex-induced vibrations in the range of wind velocities between approximately 5 and 15 m/s (10 to 35 mph).

2.1.2.1 Straight Support Standards Susceptibility to Vortex Shedding

Before describing the susceptibility to vortex shedding of the different mode shapes of the luminaire support standards the definition of the mode numbers needs to

10

be clarified. There is often a difference between the actual mode number and what is often referred to as "second mode" and "third mode". These later terms are commonly used to describe the groups of modes that put the poles into double or triple curvature, respectively. This report will use the actual mode number because it is the correct one.

Although there has been evidence in the past that vortex shedding is not a problem for most types of highway support structures it is believed to have played a potential role in the failure of the luminaire support standards along Route 147. Due to the dynamic characteristics of most highway support structures, vortex induced vibration is not typical in the first mode because the critical wind velocity is below 5 m/s. As was explained above this will generate a force with insufficient magnitude to excite the structure. First mode vibration is where most of the experimental data has been carried out on these types of structures. Higher modes may occur at frequencies that would be more conducive to vortex-induced vibrations. Table 2-1 is a summary of the first four modes of the straight support standard along Route 147. The critical velocities were calculated using Equation 2-7. Because the straight support standard is perfectly symmetric the mode shapes come in pairs for a three dimensional analysis. In other words, the first and second mode shapes are the same, the third and fourth are the same, and so on, therefore only every other mode number is discussed. Figure 2-1 shows the first mode shape of the straight support standard. As can be seen in Table 2-1 this mode would not be induced by vortex shedding because the critical wind velocity is too low.

Figure 2-2 and Figure 2-3 shows the third and fifth mode shape respectively. As can be seen in Table 2-1, the third and fifth mode shapes both have a critical velocity that is in the range that is conducive to vortex shedding. Figure 2-4 shows the straight support standard in the seventh mode shape. Table 2-1 shows that this mode would likely not occur due to vortex shedding because the critical velocity is too high.

Table 2-1 Straight Support Standard Modal Analysis Chart.		
Mode Shape	Natural Frequency	Critical Velocity (m/s)
1	0.74[*]	0.7
3	5.24	5.2
5	15.2	15.0
7	29.9	29.5

[*]Based on experimental data from pull tests, all others are based on FEA.

Hapco manufactures a damper that helps to stop second mode vibration. This damper is supposed to be standard on the 45 ft. straight support standards that were used along Route 147. Hapco has done testing on this damper by attaching it to a support standard mounted to a rigid foundation. Calculations showed that the percent of critical damping with and without the damper installed increased from 0.18% to 0.83% respectively. This amount of damping would probably increase in an actual luminaire support standard due to a less rigid base and the wires inside flapping

around. Hapco estimates that the percent of critical damping with the damper installed could increase to 2.5%, however this number is not based on results from experimental testing of an actual luminaire support standard on a foundation in second mode vibration. [8]

It is not clear how this damper will effect third mode vibration. As was discussed above, third mode vibration, in the straight support standard, is possible through vortex shedding. According to eyewitness reports by NJDOT there have been support standards that take on a third mode shape in the field. This could have been the mode that took place in the straight support standards along Route 147. It is impossible to say because no one was present to witness the supports just before failure.

2.1.2.2 Cantilevered Support Standards Susceptibility to Vortex Shedding

As was explained above, first mode vibration of the cantilevered support standards would probably not be induced by vortex shedding because the critical wind velocity is too low. Higher modes of vibration could occur however due to their higher natural frequency causing a higher critical wind velocity. Table 2-2 is a summary of the first six modes of the cantilevered support standards along Route 147. The critical velocities were calculated using Equation 2-7. Figure 2-5 shows the first mode shape of the cantilevered support standards. As can be seen in Table 2-2 this mode would not be induced by vortex shedding because the critical wind velocity is too low. The first mode of the cantilevered support standard is a twisting of the pole due to the eccentric mass of the luminaire and self-weight of the mast arm. This type of motion would probably not cause the necessary stress ranges to cause a crack at the shoe base to pole connection anyway.

Figure 2-6 and Figure 2-7 shows the second and third mode shapes of the cantilevered support standard, respectively. As can be seen in Table 2-2 these modes would not be induced by vortex shedding because their critical velocities are also too low.

Figure 2-8 shows the fourth mode shape of the cantilevered support standard. The critical wind velocity for the fourth mode shape to occur is a little low, however there have been reports from NJDOT that have suggested this mode shape has been witnessed in the field. Figure 2-9, 2-10 and 2-11 show the fifth, sixth and seventh mode shapes of the cantilevered support standard, respectively. As can be seen in Table 2-2 these mode shapes require a critical wind velocity that is capable of causing vortex-induced vibrations. As can be seen by comparing Figure 2-8 to Figure 2-10 the mode shapes for mode four and six are very similar. A slight double curvature of the pole in mode six is what distinguishes the two. It would be very easy for someone in the field to mistake mode four for mode six. Realizing this, it is probably unlikely that mode four was witnessed in the field as was reported by NJDOT. Considering the required critical wind velocity of mode four and mode six, it is more likely that the support standards were vibrating in mode six.

12

Figure 2-12 shows the eighth mode shape of the cantilevered support standard. As can be seen in Table 2-2 this mode shape has gone beyond the range for the critical wind velocity necessary for vortex shedding.

Mode Shape	Natural Frequency	Critical Velocity (m/s)
1	0.79	0.7
2	1.02*	0.9
3	1.7	1.5
4	3.9	3.5
5	7.2	7.1
6	7.5	7.4
7	10.1	10
8	16.1	15.9

Dampers are not supplied as standard items on the 40 ft. cantilevered luminaire support standards that were installed along Route 147. These particular cantilevered support standards can be outfitted with an external damper if they appear to exhibit excessive vibrations. Reports from both Hapco and NJDOT indicate that some of the cantilevered support standards along Route 147 did not have dampers installed on them at the time of the failure. These support standards would have been susceptible to any of the modes of vibration, whether due to vortex shedding or some other phenomenon that could induce vibration.

The excessive vibration of the support standards on the bridge could have been induced by the bridge itself. Support standards that are mounted on bridges have been known to exhibit excessive vibration that is induced by the bridge they are mounted to, particularly if the vibration of the bridge is in tune with one of the natural frequencies of the support standards. However, since there were also failures of poles that were not mounted to the bridge, it is unlikely that this is the primary cause of these failures. Installing a damper on any support standard that will be mounted to a bridge, no matter what the geometry of the support standard, would probably be worthwhile.

2.1.2.3 Recommended Vortex Shedding Design Loads

The current AASHTO Standard Specification for Structural Supports for Highway Signs, Luminaires, and Traffic Signals, 1994 only addresses the first mode of a non-tapered structural member for fatigue loads related to vortex shedding [9]. The methods that are used for this circumstance are correct and are applicable to the specific geometry described above. However, as has been discussed throughout this report, the susceptibility to vortex shedding goes beyond the first mode. In some

13

cases the first mode occurs at a critical wind velocity that is not conducive to vortex shedding anyway. It is necessary to calculate design loads for modes beyond the first. The Ontario Highway Bridge Design Code (OHBDC) gives an in-depth description of vortex shedding in different modes of vibration [10]. OHBDC also discusses the appropriate changes in the fatigue loads when a tapered pole is used. This code is quite complex and may be more involved than is actually needed to satisfactorily design a luminaire support standard.

2.2 Background Relevant to Fatigue Resistance of Details

Fatigue cracks can form and propagate from weld discontinuities and/or stress concentrations if a member is subjected to significant cyclic live loads, even if the maximum stresses are well below the yield strength [11, 12]. Testing on full-scale welded aluminum members has indicated that the primary effect of constant amplitude loading can be accounted for in the live-load stress range, i.e. the mean stress is not significant. The reason that the dead load has little effect on the lower bound of the results is that, locally, there are very high residual stresses in welded details. Therefore, the mean of the total stresses (applied plus residual stresses) is relatively high regardless of the dead load. In details that are not welded, such as anchor bolts, there is a strong mean stress effect. A worst-case conservative assumption, i.e. a high tensile mean stress, is made in the testing and in the design of these nonwelded details.

When structural members are tested, the loading is characterized in terms of the nominal stress in the structural member remote from the weld detail. The local stress concentration effect associated with the shape of the weld is considered part of the fatigue resistance. The nominal stress is conveniently obtained from standard design equations using member forces and moments from a global analysis.

Experience with multiaxial loading experiments on large-scale welded aluminum structural details indicates the loading perpendicular to the local notch or the weld toe dominates the fatigue life. The cyclic stress in the other direction has no effect if the stress range is below 83 MPa (12 ksi) and only a small influence above 83 MPa (12 ksi). Since the combination of multiaxial loading does not have to be considered. The recommended approach for multiaxial loads is:

1) decide which loading (primary or secondary) dominates the fatigue cracking problem (typically the loading perpendicular to the weld axis or perpendicular to where cracks have previously occurred in similar details); and,

2) perform the fatigue analysis using the stress range in this direction (i.e. ignore the stresses in the orthogonal directions) [11].

The strength and type of aluminum have only a negligible effect on the fatigue resistance expected for a particular detail. The welding process also does not typically have an effect on the fatigue resistance. The independence of the fatigue resistance from the type of aluminum greatly simplifies the development of design rules for fatigue since it eliminates the need to generate data for every type of aluminum.

14

Aluminum fatigue test data generally consist of the number of cycles to failure for a particular detail subjected to a particular constant amplitude stress range. The results are in general highly variable, therefore a statistically significant number of replicate tests must be performed. The large variance in the number of cycles to failure is primarily due to variance in both the weld geometry and weld discontinuities. This large variance makes it difficult to distinguish the secondary effects of many variables such as type of aluminum and filler metal, rate of loading, mean stress, and the environment.

Fatigue tests are performed at a number of different stress ranges and the data are generally plotted with the logarithm of the nominal stress range on the ordinate and the logarithm of the number of cycles to failure on the abscissa (even though the number of cycles is the dependent variable). The relationship used to represent the lower bound to aluminum detail test data is referred to as an S-N curve (Figure 2-13). An S-N curve is an exponential equation of the form:

$$N = C \times S^{-m} \qquad (2\text{-}8)$$

or

$$\log N = \log C - m \log S$$

where N is the number of cycles to failure, C is the constant dependent on detail category, S is the applied constant amplitude stress range, and m is the inverse of the slope of the S-N curve.

Figure 2-13 shows the constant amplitude fatigue limits (CAFL) of aluminum for each category as horizontal dashed lines. When constant amplitude tests are performed at stress ranges below the CAFL, noticeable cracking does not occur. Luminaire support structures experience what is known as long-life variable-amplitude loading, i.e. very large numbers of random amplitude cycles greater than the number of cycles associated with the CAFL. In this case, the fatigue design consists of making sure that the upper bound stress range, as defined by the recommended fatigue design load ranges, is less than the CAFL. If this is true, than the fatigue life should be essentially infinite.
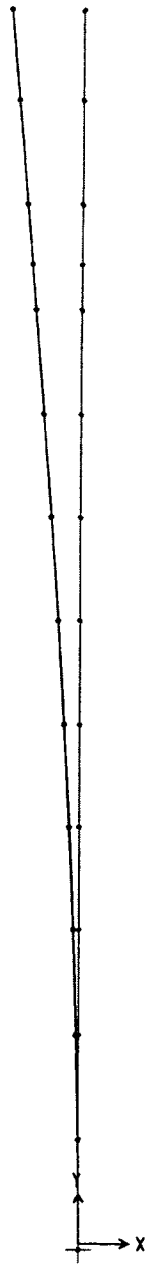
15

Figure 2-1 Straight Support Standard First Mode Shape.

16

Figure 2-2 Straight Support Standard Third Mode Shape.
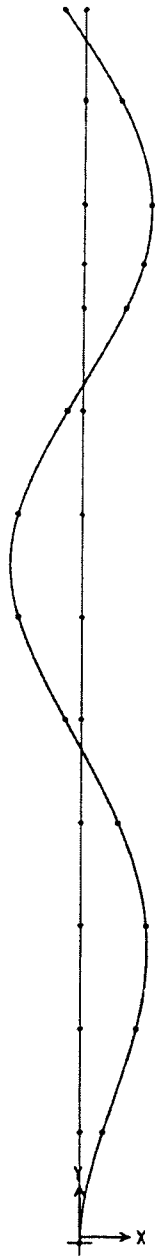
Figure 2-3 Straight Support Standard Fifth Mode Shape.

18

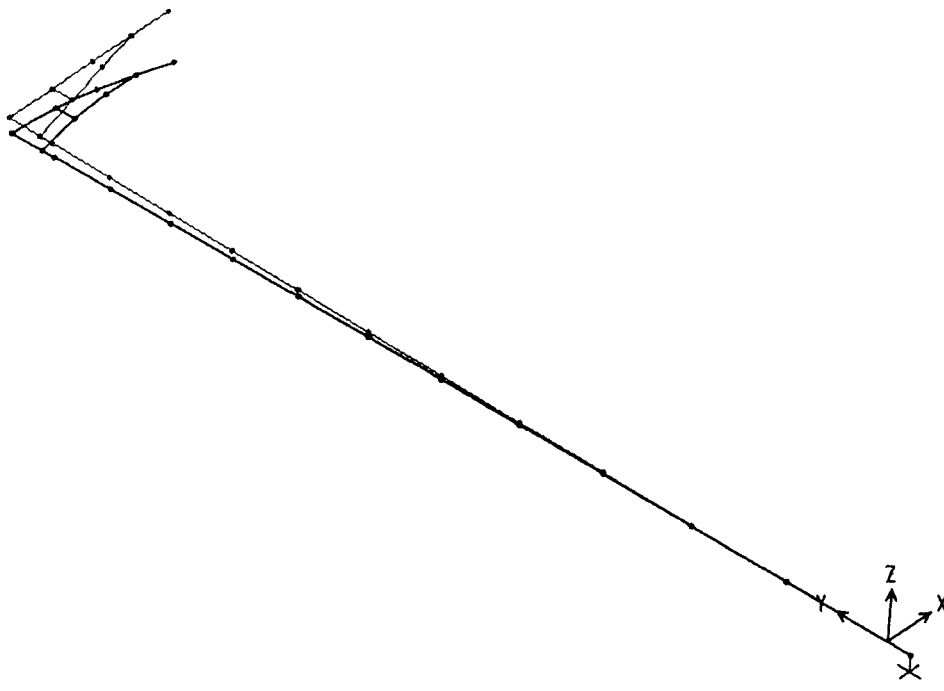Figure 2-4 Straight Support Standard Seventh Mode Shape.

19

Figure 2-5 Cantilevered Support Standard First Mode Shape.
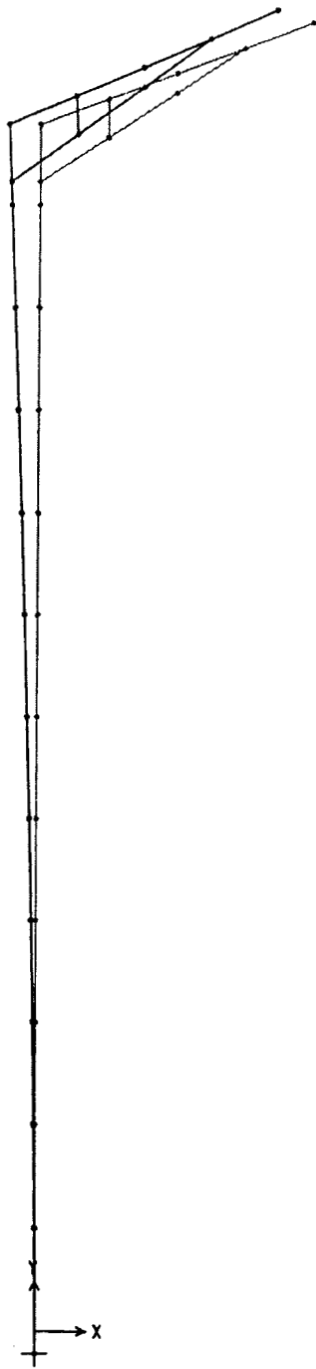
20

Figure 2-6 Cantilevered Support Standard Second Mode Shape.
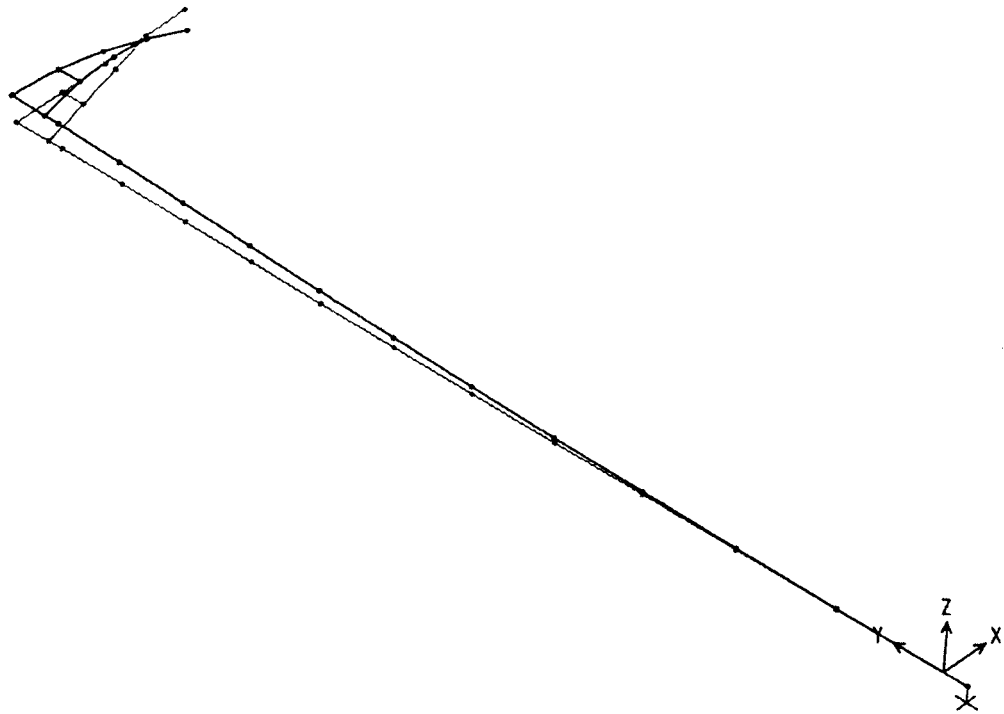
21

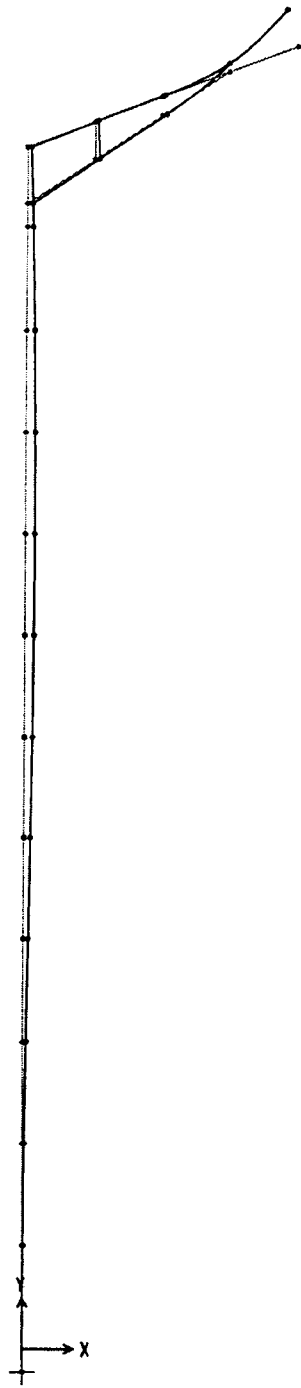Figure 2-7 Cantilevered Support Standard Third Mode Shape.

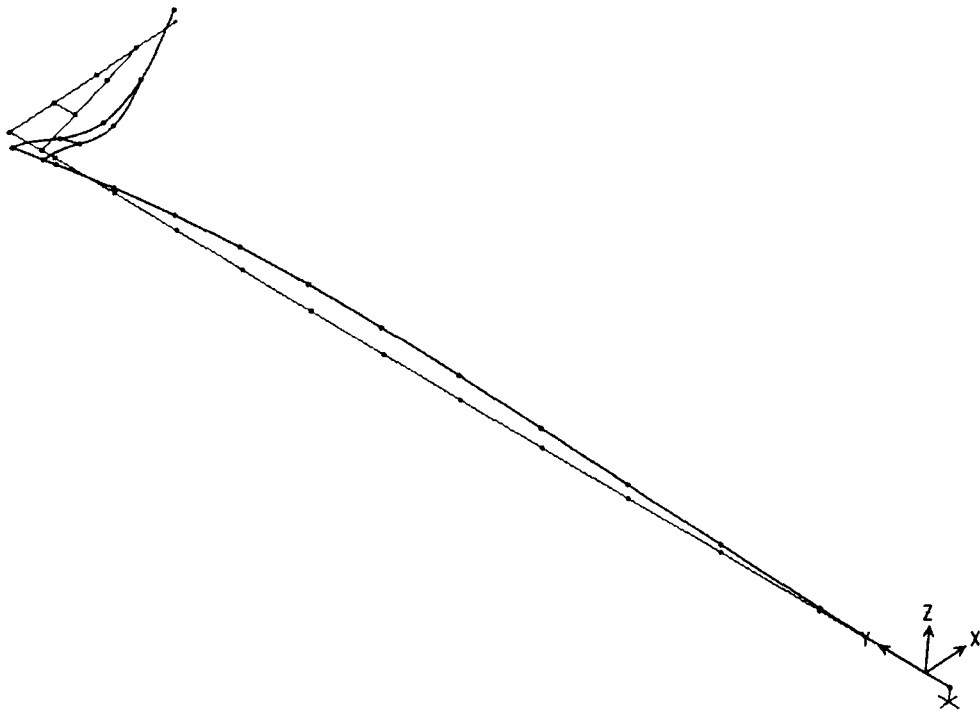Figure 2-8 Cantilevered Support Standard Fourth Mode Shape.

23

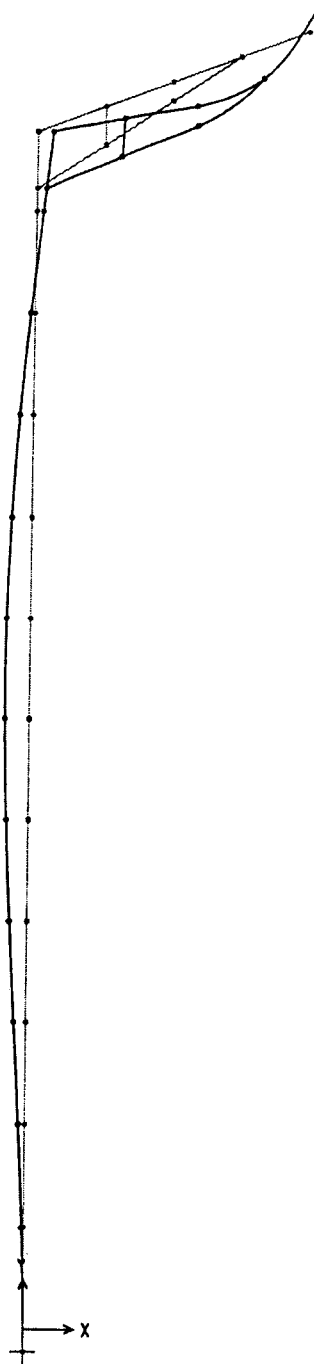Figure 2-9 Cantilevered Support Standard Fifth Mode Shape.

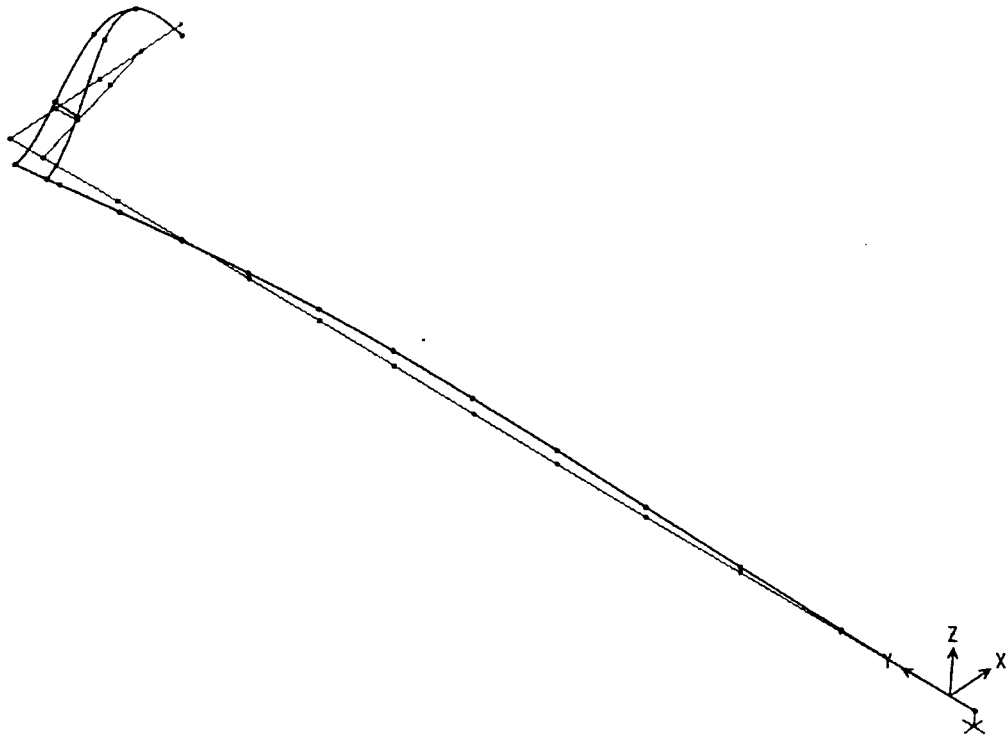Figure 2-10 Cantilevered Support Standard Sixth Mode Shape.

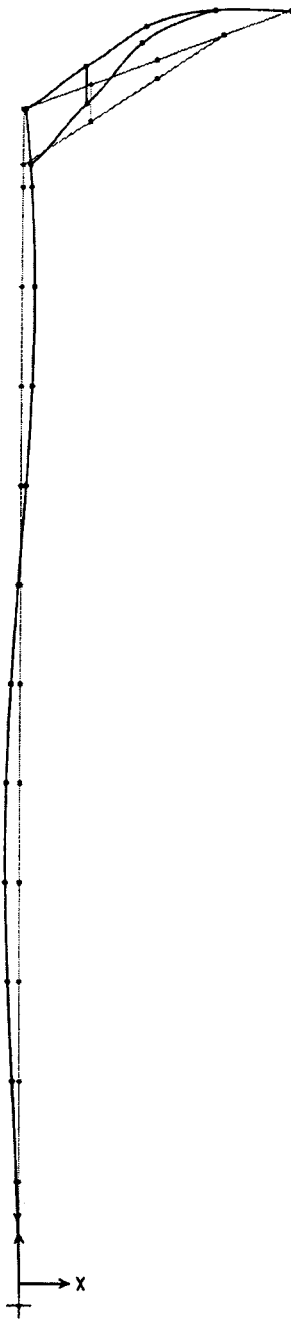Figure 2-11 Cantilevered Support Standard Seventh Mode Shape.

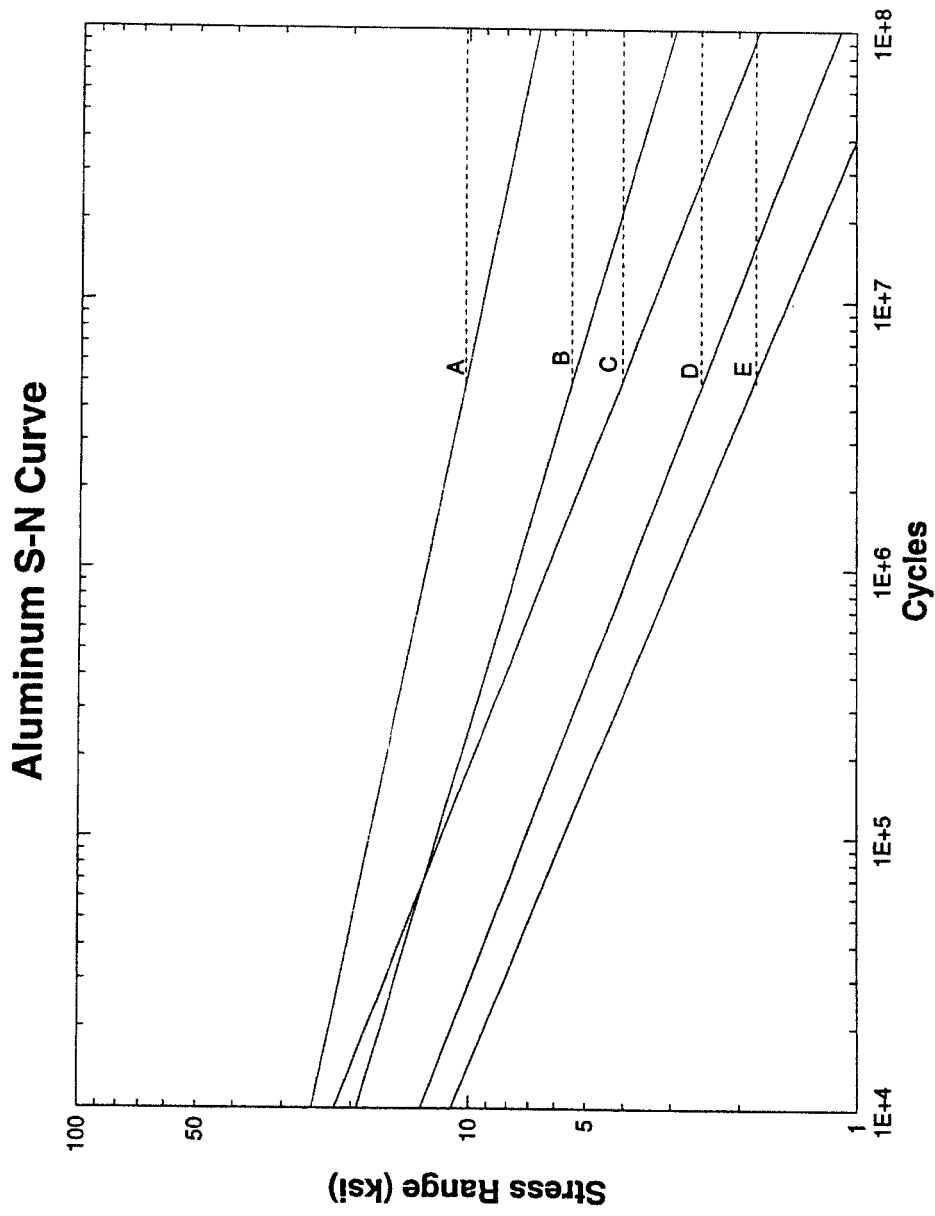Figure 2-12 Cantilevered Support Standard Eighth Mode Shape.

27

Figure 2-13 S-N Curves for Aluminum.

Chapter 3 –Testing and Findings

3.1 History of the New Jersey Luminaire Support Standards

The aluminum luminaire support standards that failed were located in southern New Jersey on Route 147. The cantilevered support standards were mounted directly to the parapet of the Grassy Sound Bridge, which is part of Route 147. These support standards experienced cracking around the shoe base-to-pole weld and at the welds around the hand access holes. The straight support standards were used along the side of the road leading up to the bridge. Only the straight support standards were connected to their foundation through the break away transformer base. All of the poles that were on a transformer base experienced failure through the transformer base and not in the pole or shoe base.

Figure 3-1 is a transformer base that was cracked alongside Route 147. In the event of an impact by a motorist, these bases are intended to break off at the tabs on the bottom where they bolt to their foundation. These breakaway tabs would seem to be the location of some of the failures since they are designed to be the weak link in the transformer base, however none of the bases appeared to fracture there. A video of the failure site taken by Hapco the next morning provided a means to view some of the failures [14].

The videotape was a valuable tool in examining the failures. Many of the cracks in the transformer bases occurred at the top where the shoe base bolted on (Figure 3-2). This may have been partly due to an error at the time the support standards were erected. Figure 3-3 describes the proper hardware, as specified by the manufacturer, to install the transformer bases. In many cases the heavy half-inch thick galvanized steel washer that helps to stiffen the transformer base around the long-slotted bolt holes were not installed. According to Hapco this leads to approximately a 50% reduction in the strength of the transformer base.

A second observation from the videotape was the lack of any significant oxidation at any of the failure surfaces. This would tend to indicate that the fatigue cracks had not been present for too long before failure occurred. A fractographic examination of a failed shoe base and transformer base indicated that the cracks did grow at a very high rate after initiation [15].

It is suspected that the support standards may have entered a mode of vibration other than first mode on the night of their failures. It was reported by Hapco and NJDOT that many of the cantilevered support standards did not have a damper installed on them. Dampers are only standard on the 45 ft. straight support standards; the other support standards are fitted with dampers only if they exhibit excessive vibrations. These dampers have only been proven effective on the second mode of vibration of a straight support standard and may have not had any effect if a higher mode of vibration were achieved.

3.2 Pull Test Description

A pull test was performed on both the cantilevered and straight luminaire support standards to determine the dynamic characteristics such as stiffness, natural frequency, and percent of critical damping

Figure 3-4 shows a straight support standard that has been positioned for a pull test. A rope was looped around the support 34 ft. up from the shoe base, which was just below the bottom part of the mast arm on the cantilevered support standards. The rope was looped around in a manner that would allow it to fall off the support standard when released so as not to add any additional damping to the system. The rope was hooked to a quick release device to allow an almost instantaneous release of the support standard. The support standard was ratcheted back by a come-along that was connected to a rigid frame. A small load cell was calibrated and placed between the come-along and quick release device. A string pot was connected to the specimen at the same location the load was applied. The string pot was disconnected from the support standard before being released with the quick release mechanism, so as not to add any additional damping to the system. With the combination of load from the load cell and deflection from the string pot a stiffness for the system could be calculated. Strain gages were attached to the support standard so a decay of motion could be recorded. A natural frequency can be extracted from the strain gage data by performing a Fast Fourier Transform (FFT).

3.2.1 Cantilevered Support Standards Pull Test Results

The pull test enabled the dynamic characteristics, such as the stiffness, natural frequency, and percent of critical damping to be calculated. Figure 3-5 shows a plot of load versus displacement. Based on this plot a stiffness of 3.6 N/mm can be calculated. A finite element analysis gives a stiffness of 3.4 N/mm. This is an excellent agreement between the FEM model and experimental data.

A Fast Fourier Transform was performed on data from a strain gage while the support standard oscillated at its second mode natural frequency. As was mentioned before, the first mode of the cantilevered support standards is twisting of the pole and is not relevant to fatigue. The natural frequency in the second mode was 1.02 cycles/s (Figure 3-6). Finite element analysis indicated a second mode frequency of 1.04 cycles/s. As with the stiffness this is an excellent agreement.

The log-decrement equation, Equation 3-1, was used to determine the percent of critical damping in the support structure

$$\frac{1}{j} \ln \frac{u_1}{u_{1+j}} = \frac{2\pi\zeta}{\sqrt{1-\zeta^2}} \qquad (3-1)$$

where j is the number of cycles being considered, u_1 is the amplitude at peak 1, u_{1+j} is the amplitude j cycles later, and ζ is the damping ratio. The percent of critical

30

damping of the cantilevered support standard was calculated with and with out the damper attached. Figure 3-7 shows the decay of motion in a strain gage when the damper was not installed. This plot represents the motion of the cantilevered support standard in its second mode. Without a damper the percent of critical damping is 0.40 percent.

Figure 3-8 shows the decay of motion in the same strain gage with the damper attached. The percent of critical damping with the damper installed is 0.41 percent. The damper does not do anything to mitigate vibration in the cantilevered support standard's second mode. The manufacturer of the damper does not claim that the damper is effective in this mode. The manufacturer openly admits that the damper is intended to mitigate only the mode shape that results in double curvature, whatever actual mode number that is for the particular structure being analyzed.

3.2.2 Straight Support Standard Pull Test Results

Finite element analysis of the straight support standard indicated a stiffness of 3.6 N/mm. The straight support standard is 5 ft taller than the cantilevered support standard, however their diameter and wall thickness is the same. Therefore it would only make sense that the stiffness of the straight support standard would almost be identical to the cantilevered, as it is.

As with the cantilevered support standard a Fast Fourier Transform was performed on data from a strain gage while the support standard oscillated at its second mode natural frequency. Because the straight support standard is perfectly symmetric the mode shapes come in pairs for a three dimensional analysis. In other words, the first and second mode shapes are the same, the third and fourth are the same, and so on. The natural frequency in the first mode was 0.74 cycles/s (Figure 3-9). Finite element analysis indicated a first mode frequency of 0.85 cycles/s. This is only a 16 percent error between the experimental data and the FEM analysis. This error could be attributed to the behavior of the pole due to the splice in the straight support standards that is not present in the cantilevers.

The percent of critical damping was calculated using Equation 3-1. The percent of critical damping for the straight support standards was 1.00 percent. Figure 3-10 shows the decay of motion in a strain gage on the straight support standard. This is over twice that of the cantilevered support standard. The 45 ft straight support comes standard with an internal damper so it was impossible to test this support standard with and without the damper. The damper should have little or no effect on this first mode of the straight support standard anyway. The additional damping in the straight support standard is probably from some mechanical damping that does not exist in the cantilevered support standard. Two sources of this mechanical damping are the lap splice in the pole and the transformer base that the pole is mounted to.

31

3.3 Fatigue Test Procedure

A fatigue test was performed on six cantilevered support standards and six straight support standards. A cantilevered and straight support standard was both bolted to the concrete foundation. The two support standards were connected together with a pinned linkage (Figure 3-11). This enabled the two support standards to be cycled at the same time. A hydraulic actuator was connected to the support standard closest to the reaction wall (Figure 3-12).

A constant amplitude fatigue test was carried out on the twelve support standards. A constant amplitude fatigue test should be performed in load control. If displacement control is used the specimen will always travel the same distance in each cycle. This is fine until a crack forms, then the stress range will drop off because the specimen is not traveling farther to make up for the loss in stiffness. If load control is used the specimen will travel whatever distance needed to achieve the desired stress range. Load control was a problem in this test because of the extremely low loads needed to achieve the desired stress ranges. To overcome this, control was maintained through a strain gage instead of a load cell. Both of these devises are voltage devises, therefore the controller will accept a signal from both of them. Using strain control enabled a constant amplitude stress range to be maintained even with the extremely low loads.

The stress ranges chosen in the fatigue test were intended to show two things, the magnitude of stress ranges that existed in the field on Route 147 and the threshold for the CAFL of this detail. The fractographic examination of the failed luminaires suggested a very high stress range in the field. An approximation of the stress range was unable to be performed because ΔK became to high to make striations shortly after the crack formed. Lower stress ranges were used in the fatigue test to try to pinpoint the threshold. If a specimen ran for over 2 million cycles without cracking then the next specimens would be ran at a higher stress range. If those two cracked the next two would be cycled at the mean stress range of the two previous tests. This procedure enabled the CAFL to be zeroed in on. The inherent scatter in fatigue data made finding the CAFL with such a limited number of specimens difficult.

Table 3-1 (next page) shows the stress range that each of the support standards were tested at and the condition at the time the support standard was replaced with a new specimen. In Table 3-1 a support standard number with an S-# is a straight support standard mounted on a transformer base and a C-# is a cantilevered support standard mounted directly to the foundation, with the exception of the last cantilevered support standard which was mounted on a transformer base. The stress range in the chart is the nominal stress range at the weld toe of the shoe base to pole connection. The support standards were oriented so the east and west faces saw the maximum stress range and the north and south faces were on the neutral axis. If a transformer base was used it was oriented so the access hole was on the west side, and thereby saw the maximum stress range. A specimen that is listed with a condition of a "runout" is one that developed no cracks.

32

Table 3-1 Support Standard Fatigue Test Summary			
Pole #	S_R (MPa)	Cycles (x1000)	Condition
S-1	34.5	2000	Runout
S-2	69.0	55	127 mm. crack at weld toe through pole
S-3	51.7	861	76 mm. crack weld toe through pole, 38 mm. crack in TB
S-4	38.3	2000	Runout
S-5	48.2	197	127 mm crack behind weld leg
S-6	69.0	553	229 mm crack behind weld leg, cracks in TB
C-1	64	109	76 mm crack through weld throat
C-2	51.7	515	102 mm crack at weld toe through pole
C-3	55.1	2660	Runout
C-4	84.0	36	165 mm crack at weld toe through pole
C-5	39.6	5710	Runout
*C-6	34.5	5710	Runout in pole, cracks in TB

*Only cantilevered support standard tested that was mounted to a transformer base.

3.4 Fatigue Test Results

The following sections describe the results of the fatigue test as it applied to each component of the luminaire support structure.

3.4.1 Transformer Bases

Three of the seven transformer bases included in the fatigue test developed cracks at various locations. Specimen S-3 developed a crack at the top corner of the access hole (Figure 3-13). There was a small notch that was noticeable at the origin of the crack. There appeared to be grinding marks going in two directions in the area of the crack that helped to form a point on the edge of the access hole. This combination of a sharp edge with a notch initiated the fatigue crack.

Specimen S-6 developed cracks in two places. The first crack started to form in the side of the transformer base wall opposite the access hole (Figure 3-14). After the test this crack was cut out and a definite change in thickness was noticed in the transformer base wall (Figure 3-15). The thinner wall was caused by excess grinding on the side of this transformer base. There may have also been an attempt at a weld repair in the base metal of this transformer base. Apparently there was a surface defect in this base. Instead of discarding it a repair was attempted and this was the origin of the first fatigue crack. The second crack in this base originated at the back of the finger tabs that are used to bolt the structure to its foundation (Figure 3-16). This crack appeared to originate out of the radius at the back of the finger tabs.

33

Specimen C-6 was the only cantilevered support standard mounted to a transformer base. This was simply done to try to get more data on the behavior of the transformer base. Three cracks formed in the transformer base to specimen C-6. Two of these cracks formed at the back of the finger tabs at opposite corners of the base, much the same as the transformer base to specimen S-6. It is important to ensure that this area is kept smooth and free of notches to avoid anything that can cause a stress concentration. The third crack in this specimen formed in one of the long-slotted holes at the top of the transformer base where the shoe base bolts on. Figure 3-17 shows a large casting defect near the surface at the location where the crack originated. Casting defects such as this can be common in the process that is used to make the transformer bases.

3.4.2 Pole Cracks Induced by Bending

As can be seen in Table 3-1 four of the seven cracks in the poles formed as a semi-elliptical weld toe crack that propagated through the pole and then continued on around the circumference. Figure 3-18 shows a typical fatigue crack that formed and propagated in this manner. The cracks that formed at the weld toe and propagated through the pole are plotted separately from those that cracked behind the weld toe. This is because the crack that formed behind the weld toe is primarily caused by a shear stress on the effective area of that weld leg and should consequently be compared to a Category F type detail.

There are two methods for plotting crack data on an S-N curve. One is to include the runouts in the mean minus two standard deviations calculations and the other is to leave them out. Different researchers prefer one to the other and it is not clear which is more "correct". The thing that is clear is that not including the runouts in the computation results in more conservative values for the mean minus two standard deviations calculation. Both methods are presented here for comparison of the impact on the final decision of the detail category. Figure 3-19 and Figure 3-20 show an S-N plot of the through-thickness fatigue crack data not including the runouts and including them in the mean minus two standard deviations calculation, respectively. As can be seen from comparing the two plots the mean minus two standard deviation is more conservative when the runouts are not included, however in this data set the fatigue strength of the detail is equal to Category E regardless of weather the runouts are included or not.

Previous research performed for Caltrans by Fisher et al has indicated similar results. This research was performed on a steel socket detail used in California light pole standards. Although the California standards are steel and the New Jersey standards are aluminum a comparison can still be made. The fatigue resistance of an aluminum detail is typically about one third that of the same detail made of steel. However, the magnitudes of the CAFL for the two materials are scaled to already compensate for this. Therefore, a Category E detail in steel correlates to a Category E detail in aluminum.

34

Fisher indicated that the socket detail that was tested for Caltrans had a fatigue strength equal to Category E'. The geometry of the two details was not exactly the same, which is a possible reason for the difference in fatigue strength. Considering the inherent scatter in fatigue data and the limited number of specimens in each study, the results of the two tests being this similar is not bad. The Fisher test also indicated that an unequal leg fillet weld would increase fatigue strength of the detail. When the weld leg on the pole was longer the fatigue strength was noticeably increased. Although there were only fillet welds with equal legs tested on the aluminum poles there is no reason to assume that a longer fillet would not help this detail as well [13].

3.4.3 Pole Cracks Induced by Shear

Three of the seven cracks were formed in a manner that must be compared to Category F, the category for shear stress on the weld. Two of these poles exhibited a failure that was caused by a crack that started at the weld root and quickly propagated upward to intersect a very shallow crack at the weld toe (Figure 3-21). When these specimens were cycling in the fatigue test there was no way to know the crack was forming in a different manner, however after the testing the cracks were cut open and then it was obvious. Figure 3-21 shows that the effective weld size in some locations along the tube was a small as a quarter inch. This weld is supposed to be a seven sixteenth inch weld. If this weld is made correctly the nominal stress range in the tube wall should be 1.75 times greater than the shear stress range on the fillet leg. However, if the weld is made with the effective weld size as is indicated in Figure 3-21 the shear stress range on the fillet leg becomes equal or even greater than that in the tube wall. This causes a ΔK at the weld root higher than that at the weld toe which is why the root crack quickly propagated up to intercept the toe crack before it went through thickness. This lack of fusion that causes the effective weld size to be reduced is a quality control issue that needs to be addressed.

Figure 3-22 shows a typical fatigue crack that propagated from the weld root through the weld throat. This type of crack is also cause by a shear stress range on the weld. The weld throat represents the weakest plane through the weld and is where a crack will form is one is going to propagate through the weld metal.

Figure 3-23 shows an S-N plot of the shear-induced cracks compared to category F. As can be seen in this figure when the cracks are shear induced the detail has a fatigue strength below Category F.

3.5 Comparison with Route 147 Failures

Upon completion of the fatigue test cracks from specimens C-2 and C-4 were cut open and examined under a scanning electron microscope. These two specimens were chosen because they were tested at 51.7 MPa (7.5 ksi) and 84 MPa (12.2 ksi), respectively. These stress ranges were originally thought to be close to what the stress range was when the failures occurred on Route 147. Figure 3-24 and Figure 3-

25 show striations from a fatigue crack generated in specimen C-4 during the fatigue test and a support standard that failed on Route 147, respectively. As can be seen in these figures the striations from the fatigue test are closer together, which indicates a lower stress range. It is not clear what the exact stress range was in the support standards on Route 147, but it appears to have been greater than 84 MPa (12.2 ksi). There were no specimens tested at a stress range higher than 84 MPa, therefore a closer comparison of striation spacing cannot be made.
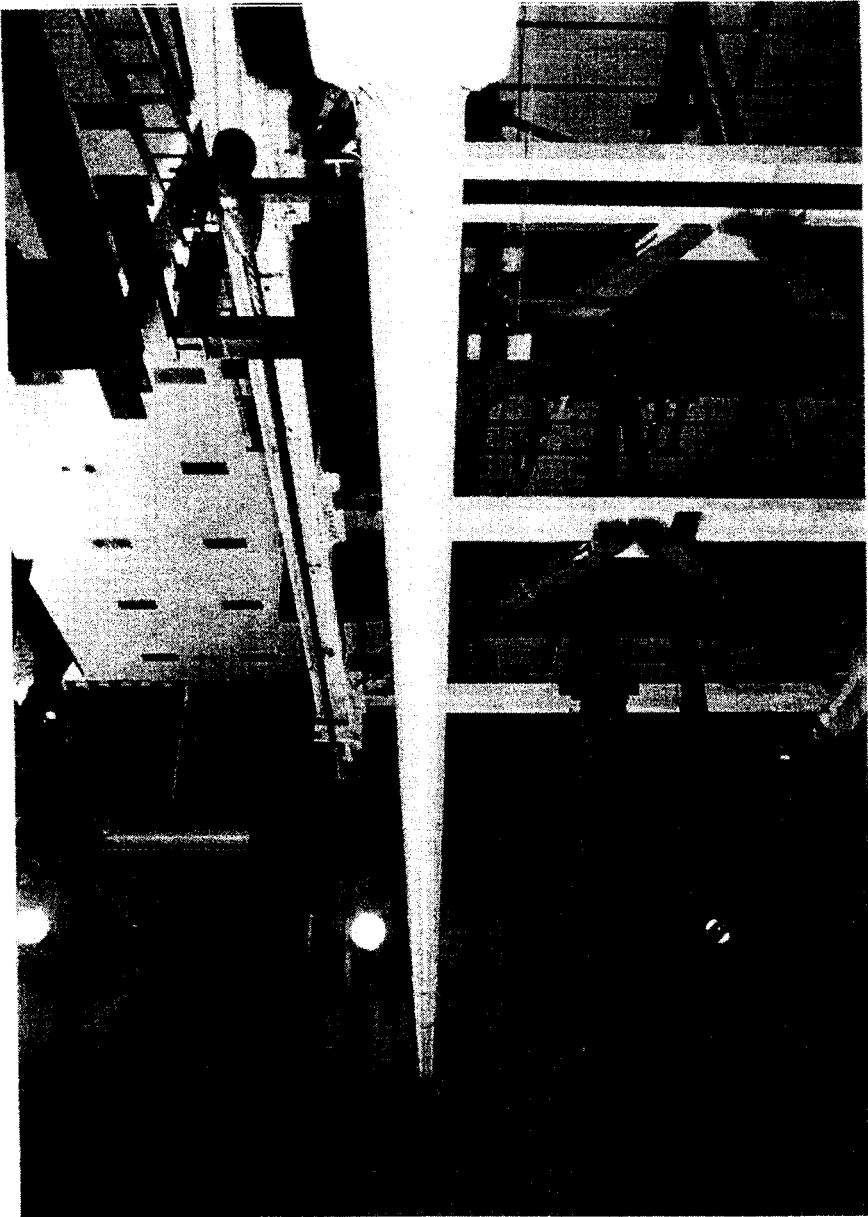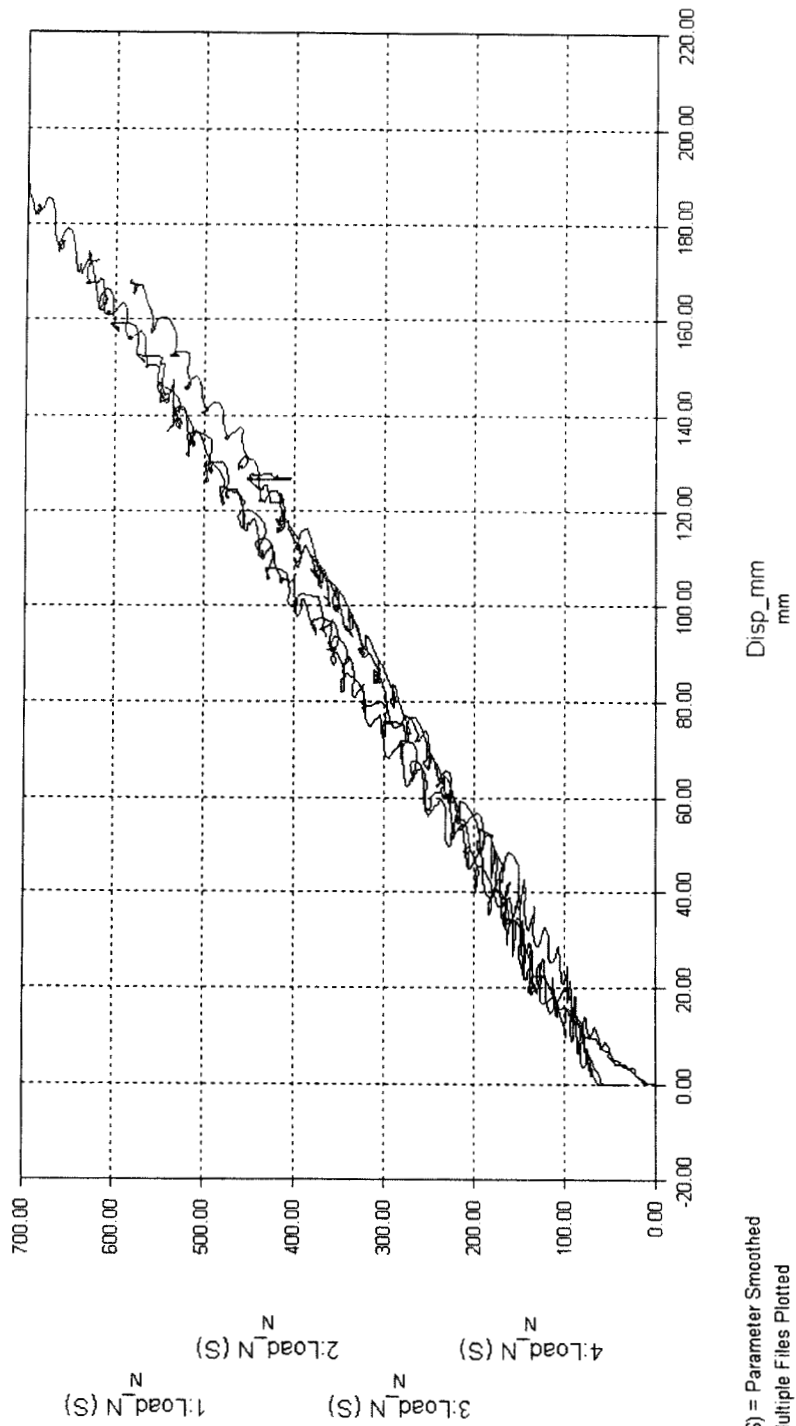
Figure 3-1 Cracked Transformer Base from Route 147.

Figure 3-2 Cracked Transformer Base where Shoe Base Bolts on.

37

Shoe base

1"-8 NC x 3" S.S
Hex Head Bolt

1" S.S. Flatwasher

17" High Lighting
Pole Breakaway
Transformer Base.

Flatwasher, Galv. Stl.
2 ¾" O.D. x ½" Thick

1" Stainless Stl. Lockwasher

1"-8NC S.S. Hex Nut

1"-8 NC x 3" S.S
Hex Head Bolt

1" Stainless Stl. Lockwasher

1" S.S. Flatwasher

Flatwasher, Galv. Stl.
2 ¾" O.D. x ½" Thick

1" Hexagon Coupling,
Galv. Stl.

1"-8NC x 36" Galv.
Stl. Anchor Bolt

Figure 3-3 Transformer Base Mounting Procedure

38

Figure 3-4 Straight Support Standard Positioned for Pull Test.

Stiffness of Cantilevered Support

Figure 3-5 Stiffness of Cantilevered Support

Disp_mm
mm

700.00
600.00
500.00
400.00
300.00
200.00
100.00
0.00

-20.00 0.00 20.00 40.00 60.00 80.00 100.00 120.00 140.00 160.00 180.00 200.00 220.00

1:Load_N (S)
N

3:Load_N (S)
N

2:Load_N (S)
N

4:Load_N (S)
N

(S) = Parameter Smoothed
Multiple Files Plotted

Amplitude Spectrum of sg1   Time: 73.05 to 175.50
FFT Size: 2048   FFT Window Type: Rectangle/None
Peak of 158960.62 at 1.02 Hz.
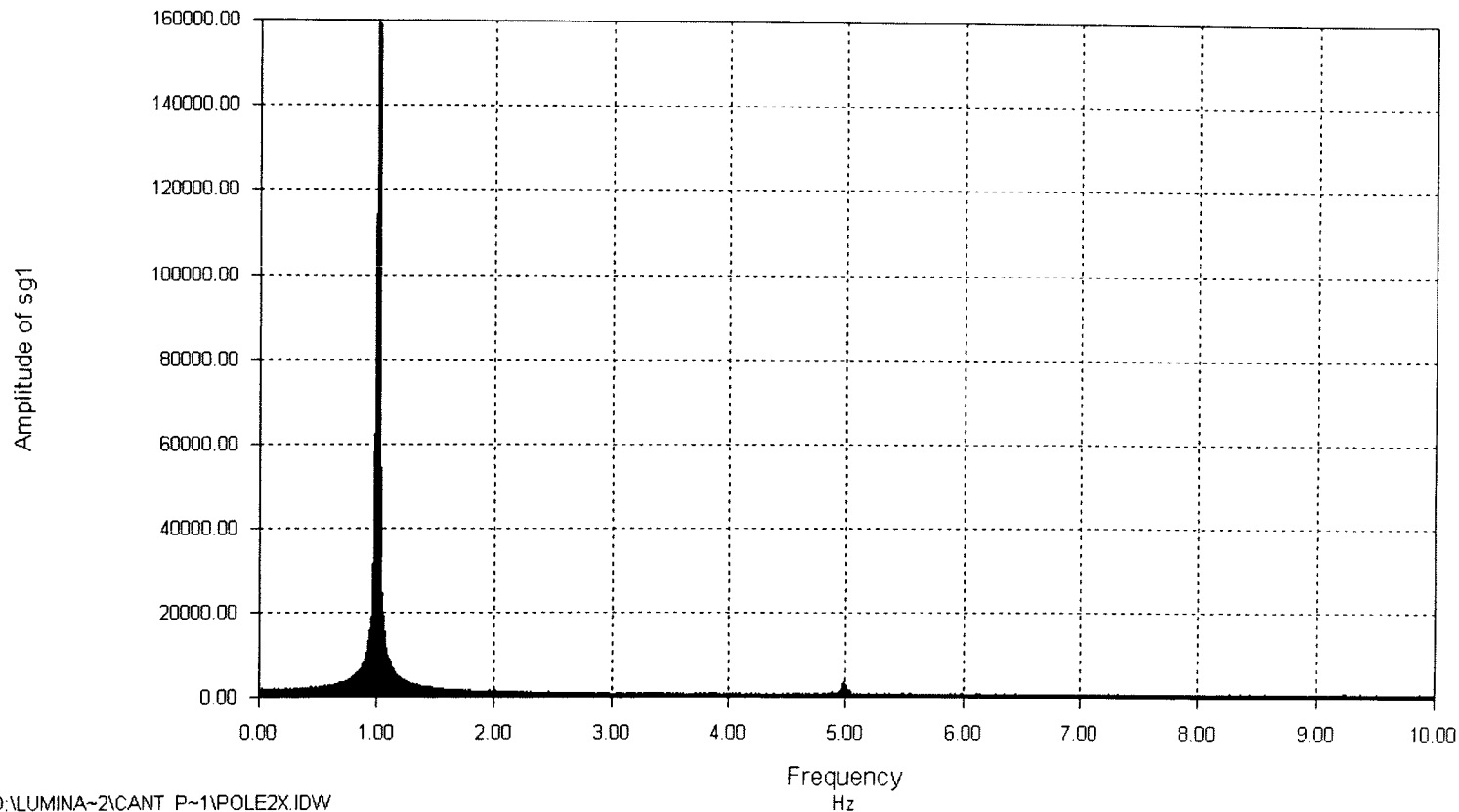
Figure 3-6 Natural Frequency of Cantilevered Support

D:\LUMINA~2\CANT_P~1\POLE2X.IDW

Cantilevered Support without Damper

(S) = Parameter Smoothed
D:\LUMINA~2\CANT_P~1\POLE2X.IDW
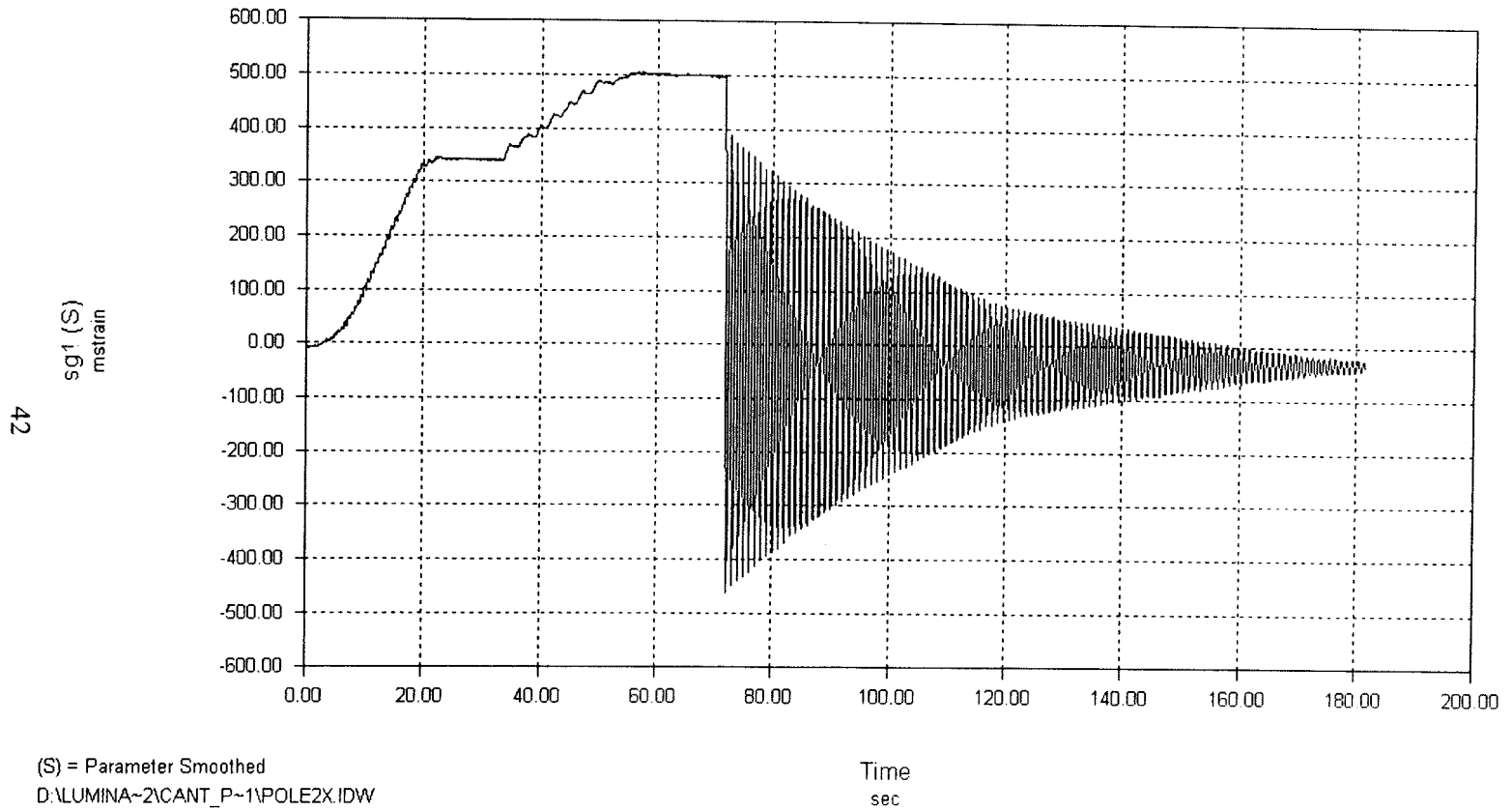
Figure 3-7 Damping of Cantilevered Support with No Damper

Cantilevered Support with Damper

Y-axis label: sg1 (S) mstrain

Y-axis values: 500.00, 400.00, 300.00, 200.00, 100.00, 0.00, -100.00, -200.00, -300.00, -400.00, -500.00, -600.00

X-axis values: 0.00, 20.00, 40.00, 60.00, 80.00, 100.00, 120.00, 140.00, 160.00

(S) = Parameter Smoothed
D:\LUMINA~2\CANT_P~1\POLE3X.IDW
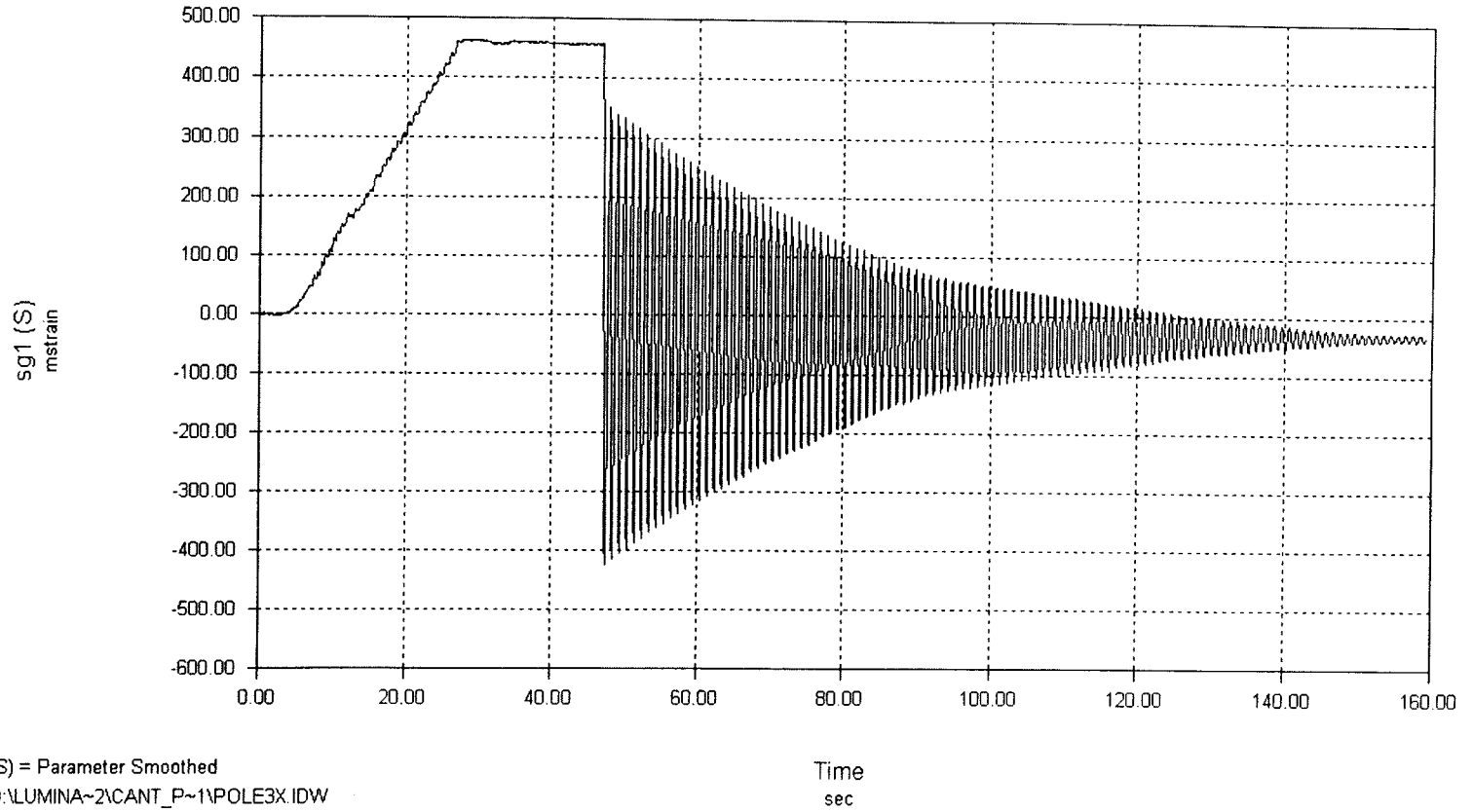
Time
sec

Figure 3-8 Damping of Cantilevered Support with Damper

43

Amplitude Spectrum of sg2 Time: 49.48 to 100.70
FFT Size: 2048   FFT Window Type: Rectangle/None
Peak of 162797.53 at 0.74 Hz.
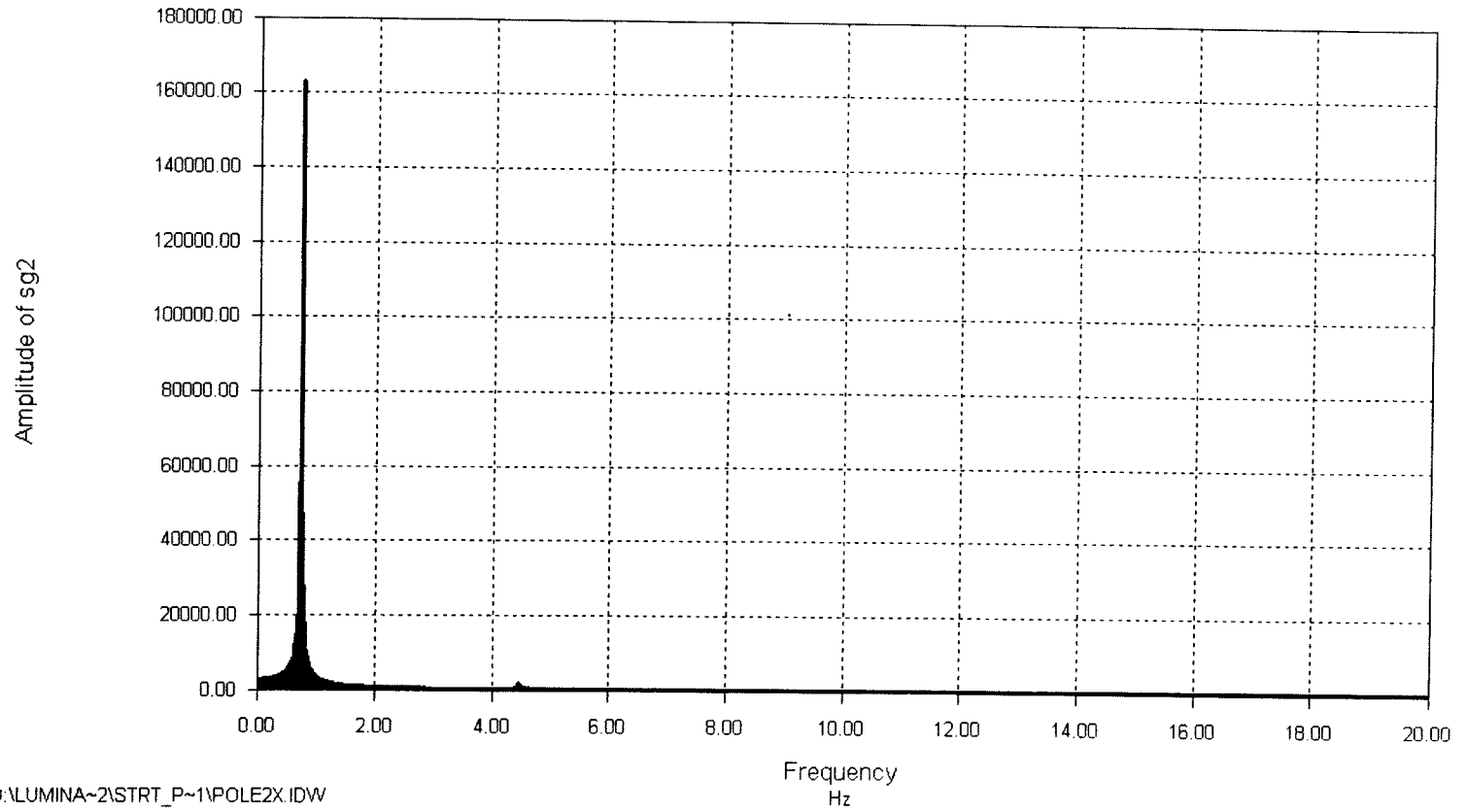
D:\LUMINA~2\STRT_P~1\POLE2X.IDW

Figure 3-9 Natural Frequency of Straight Support

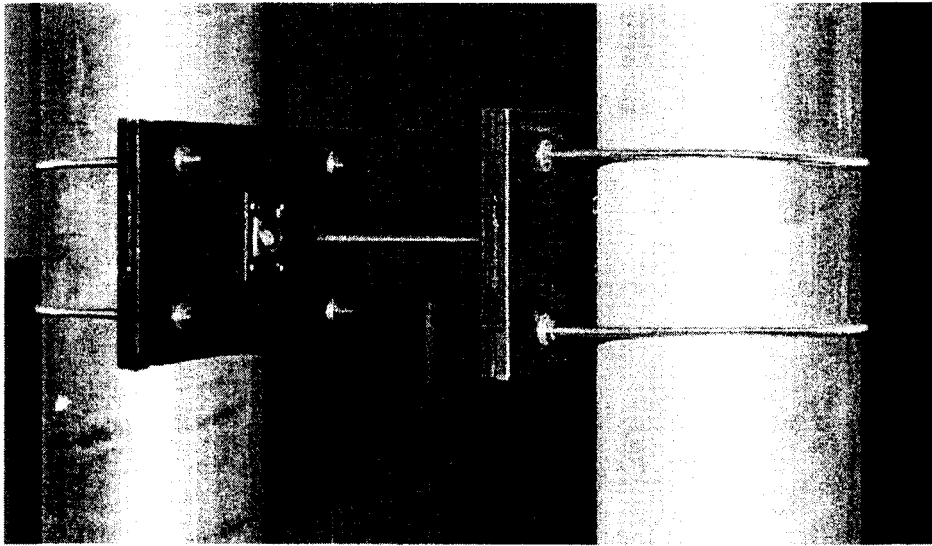Figure 3-10 Damping of Motion in a Straight Support

45

Figure 3-11 Linkage to Connect Support Standards in Fatigue Test

Figure 3-12 Actuator used in Fatigue Test

Figure 3-13 Fatigue Crack in Transformer Base of Specimen S-3

Figure 3-14 Fatigue Crack in Wall of Transformer Base of Specimen S-6

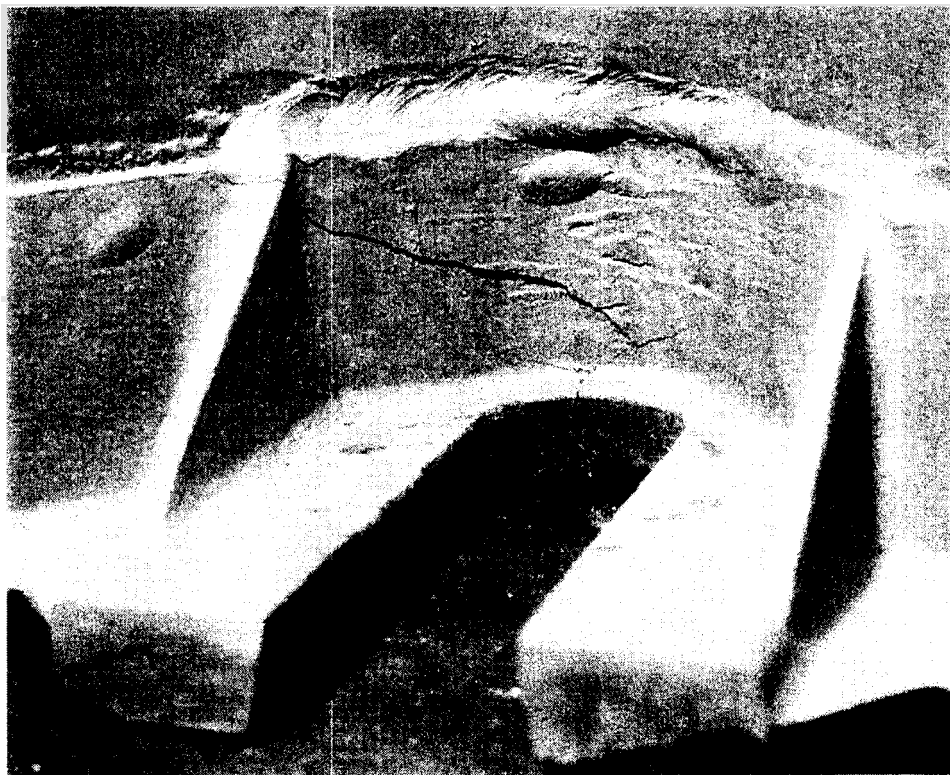Figure 3-15 Cross Section of Transformer Base Wall of Specimen S-6

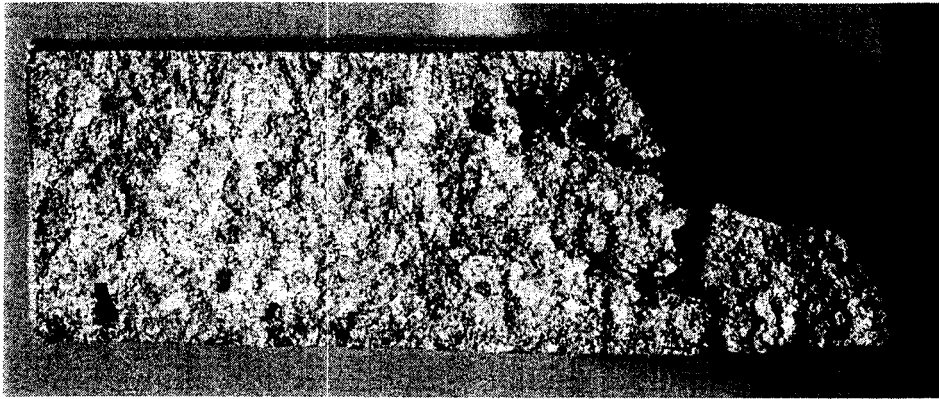Figure 3-16 Fatigue Crack in Finger Tabs of Transformer Base of Specimen S-6

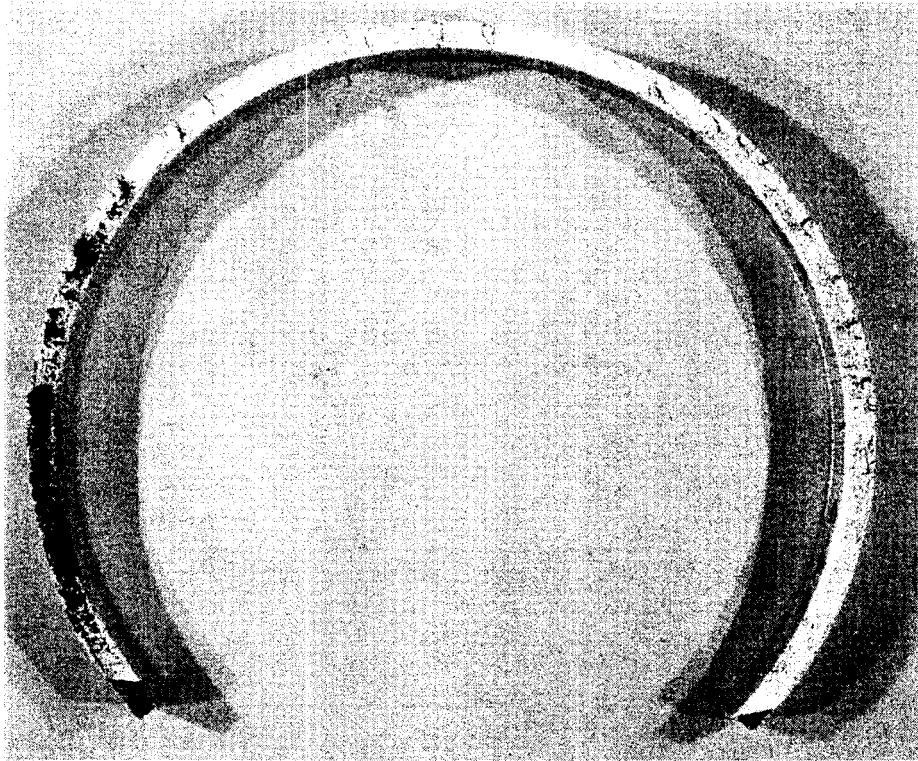Figure 3-17 Large Casting Defect in Transformer Base of Specimen C-6.

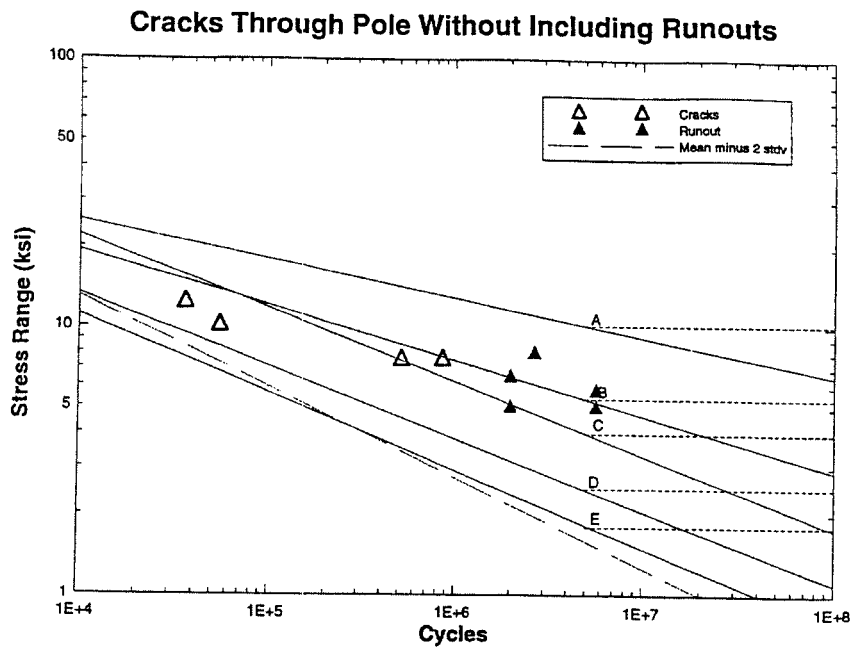Figure 3-18 Typical Through-Thickness Weld Toe Crack.

Cracks Through Pole Without Including Runouts

Figure 3-19 S-N Curve for Through-Thickness Cracks Not Including the Runouts.
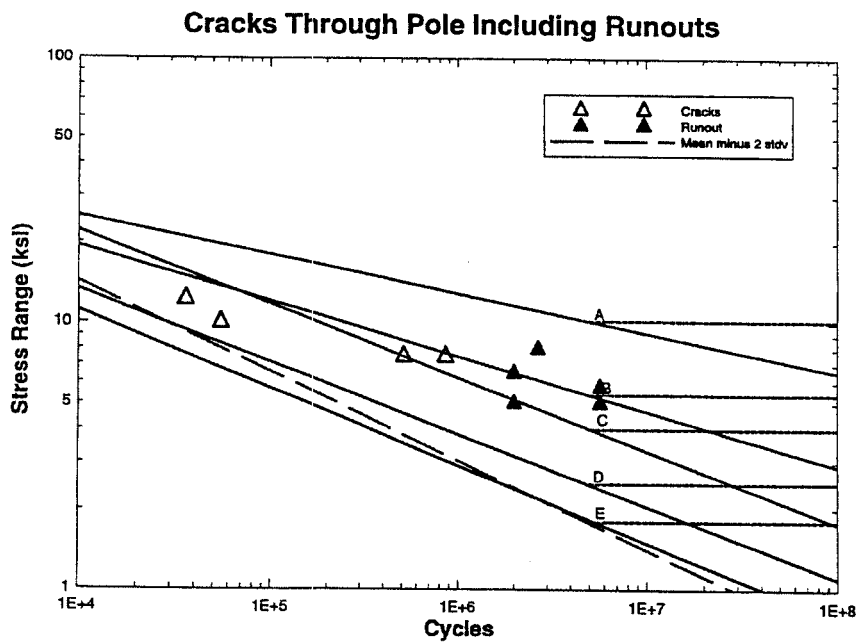
Cracks Through Pole Including Runouts

Figure 3-20 S-N Curve for Through-Thickness Cracks Including the Runouts.
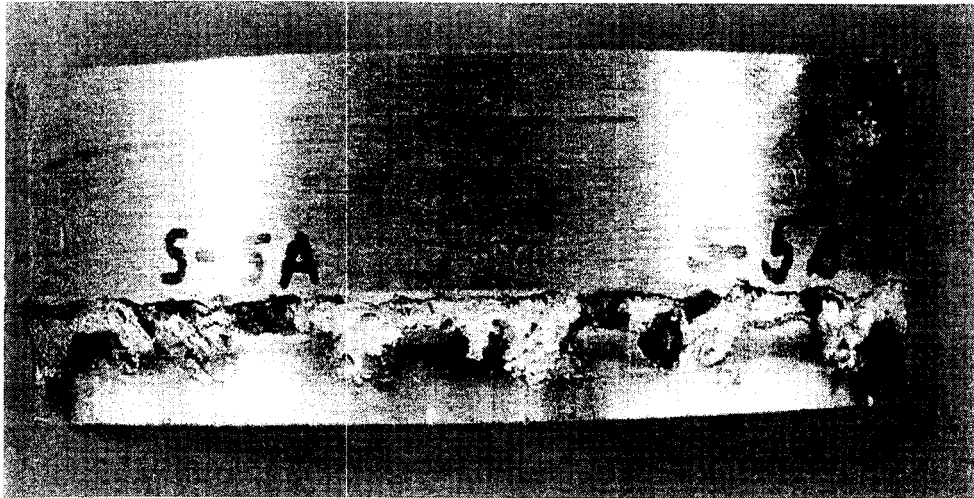
50

Figure 3-21 Typical Fatigue Crack that Propagates from Behind the Weld Leg.

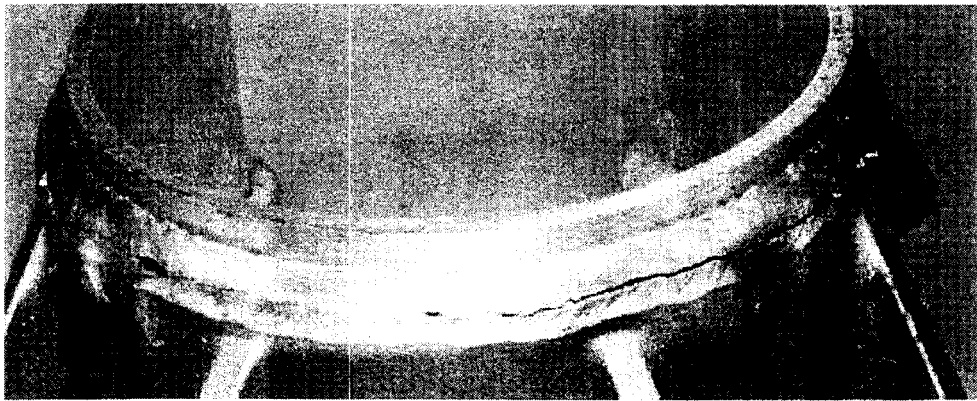Figure 3-22 Typical Fatigue Crack that Propagates Through the Weld Throat

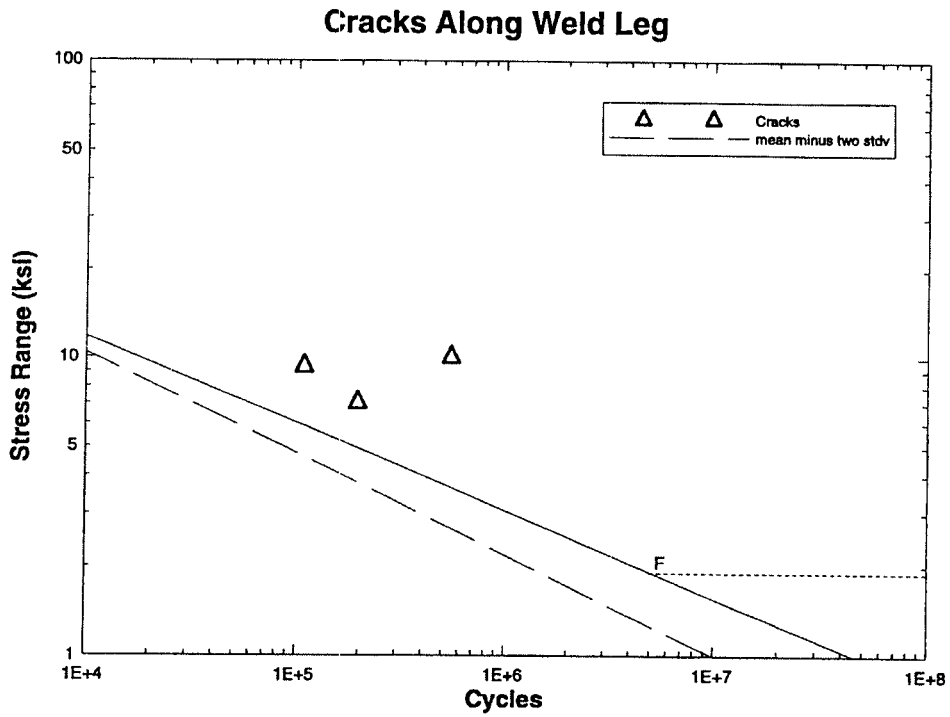**Cracks Along Weld Leg**

Figure 3-23 S-N Curve for Shear Stress Range Induced Cracks
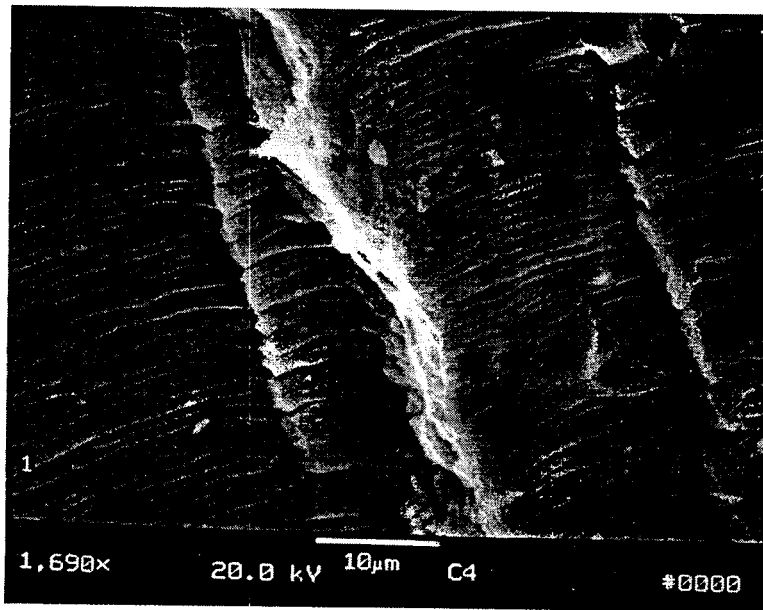
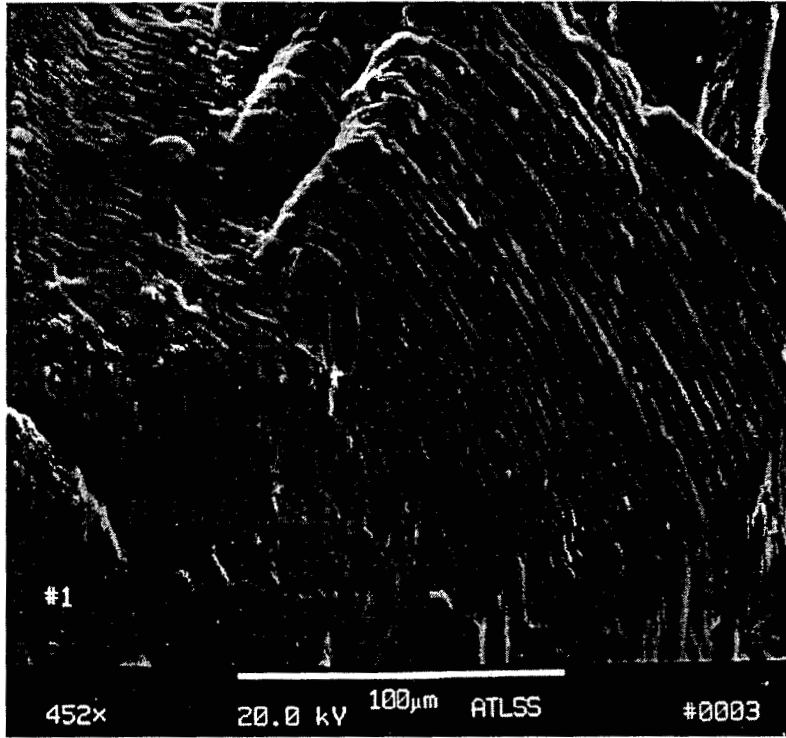

Figure 3-24 Striations in Specimen C-4.

Figure 3-25 Striations from Cracked Pole on Route 147.

Chapter 4 – Conclusions and Recommendations

4.1 Conclusions from Fatigue Testing

The following conclusions were drawn from the fatigue test of twelve aluminum luminaire support standards.

- The fatigue strength of the shoe base detail was equal to Category E.

- Several transformer bases developed cracks in multiple areas. Casting defects and notches in the base metal caused most of these cracks. The fatigue strength of these details is difficult to quantify since the stress ranges are not well defined at these locations.

- The highest stress range of 84 MPa (12.2 ksi) that a specimen was tested at was determined to be less than the stress ranges experienced on Route 147. The exact stress range that the failed poles experienced on Route 147 was impossible to determine from a fractographic examination, however the appearance of the fracture surface indicated the stress range was larger than 84 MPa.

4.2 Design Recommendations

The results of the research contained herein indicate that the following fatigue design loads and improved details should be used for luminaire support structures.

4.2.1 Natural Wind Gusts

Natural wind gusts are a concern for all types of highway support structures. These structures could be designed for fatigue from natural wind gusts with the following loads.

- All types of cantilevered sign and luminaire support structures could be designed for natural-wind-gust loads using an equivalent static pressure range of 250 Pa (5.2 psf) times the drag coefficient which is applied horizontally to the horizontally projected area of any exposed portions of the structure and the attachments. Equation 4-1 indicates the appropriate pressure from natural wind gusts

$$P_{NW} = 250C_dI_F \qquad \text{(Pa)} \qquad (4\text{-}1)$$

54

where C_d is the appropriate drag coefficient from table 1.2.5C of the AASHTO specification and I_F is the importance factor based on the sign environment.

4.2.2 Vortex Shedding

Vortex shedding is a concern for symmetric, prismatic structures such as luminaire support standards. These structures could be designed for fatigue from vortex shedding with the following loads.

- Perform a finite element analysis to determine the appropriate natural frequencies and mode shapes of the structure. The appropriate natural frequencies are those that when used in Equation 4-2 result in a critical wind velocity, V_{cr} (m/s), between 5 and 15 m/s.

$$V_{cr} = \frac{f_n D}{S} \qquad (4\text{-}2)$$

where f_n is the natural frequency of the structure, D (m) is the average diameter of the pole, and S is the Strouhal number. The appropriate Strouhal number for luminaire support structures is 0.18.

- Use Equation 4-3 to compute the appropriate pressure to apply to each of the mode shapes.

$$P_{VS} = \frac{0.613\left(V_{cr}^2\right)C_d I_F}{2\zeta} \qquad (4\text{-}3)$$

where P_{VS} (Pa) is the vortex shedding pressure, V_{cr} (m/s) is the critical wind velocity, C_d is the appropriate drag coefficient from Table 1.2.5C of the AASHTO Code, I_F is the Importance factor based on the location of the structure, and ζ is the damping ratio conservatively estimated at 0.005 unless experimental data can give more accurate results.

- Apply the vortex shedding pressures to their appropriate mode shapes from the finite element analysis. Apply the pressure in the direction that the support standard is displaced, based on the mode shape from FEA.

For an example of the application of vortex shedding to a tapered luminaire support standard see Appendix A.

4.2.3 Improved Shoe Base-to-Pole Connection

Improvements in the shoe base-to-pole connection could be made by following these suggestions.

- Bevel the inside top edge of the shoe base. This will result in a larger weld leg along the pole, thereby reducing the shear stress on the weld.

- Use an unequal leg fillet on the top of the shoe base. This will result in a larger weld leg along the pole, thereby reducing the shear stress on the weld.

- Increase the pole diameter and/or thickness. This will increase the section modulus, thereby reducing the nominal bending stress in the pole.

- Use steel rather than aluminum.

Any or all of these suggestions should help to better the shoe base-to-socket detail.

4.2.4 Installation Procedure

There were reports that many of the heavy washers required for the transformer base to achieve its full strength were missing at the failure on Route 147 (Figure 3-3). In the video of the failure scene, shot by Hapco, there was some cracking noticed in the long-slotted holes that the shoe base mounts to. It is imperative that the manufacturer's guidelines be followed to develop the full strength of all the components of the luminaire support system. The manufacturer supplies a set of installation procedures with the support standards that should be followed to guarantee maximum performance.

References

1. Kaczinski, M.R., et al., <u>Fatigue-Resistance Design of Cantilevered Signal, Sign, and Light Supports</u>, National Cooperative Highway Research Program, Final Report - NCHRP Project 10-38, Transportation Research Board, Washington D.C., 1996.

2. Davenport, A.G., The Spectrum of Horizontal Gustness Near the Ground in High Winds, Quarterly Journal, Royal Meteorological Society Vol. 87, London 1961.

3. Lundquist, R.C., et al., Aerodynamically Induced Stresses in Traffic Signals and Luminaire Supports, Mechanics Research Report MRI-TR-2430-1, Bridge Department, California Division of Highways, 1972.

4. Liu, H., Wind Engineering - A Handbook for Structural Engineers, Prentice Hall, Englewood Cliffs, NJ, 1991.

5. Simiu E., et al., Wind Effects on Structures: An Introduction to Wind Engineering, John Wiley & Sons, NY, 1996.

6. Blevins, R.D., <u>Flow-Induced Vibration</u>, Second Edition, Van Nostrand Reinhold, New York, NY, 1990.

7. Kolousek, V., et al., <u>Wind Effects on Civil Engineering Structures</u>, Elsevier, New York, NY, 1984.

8. Minor, R. C., "Structural Damping Coefficient using Hapco Vibration Damper", Hapco Report, Hapco Co., Abingdon, VA, June 9, 1994.

9. AASHTO, <u>Standard Specifications for Structural Supports for Highway Signs, Luminaires and Traffic Signals</u>, The American Association of State Highway and Transportation Officials, Washington D.C., 1994.

10. <u>Ontario Highway Bridge Design Code, Third edition,</u> Ministry of Transportation, Downsview, Ontario, 1992.

11. Dexter, R. J. and Fisher J. W., Fatigue and Fracture – Chapter 8, <u>Steel Design Handbook LRFD Method</u>, Tamboli, A. R. (ed.), McGraw Hill, 1997.

12. Dexter R. J., and Fisher J. W., Fatigue and Fracture - Chapter 24, <u>Handbook of Structural Engineering,</u> Chen, W. S. (ed.), CRC Press LLC, Boca Raton, FL, 1997.

13. Fisher, J. W., et al, <u>Fatigue Behavior of Steel Light Poles</u>, Caltrans, December 1981.

14. Mantz, H., "New Jersey DoT Pole Failures", Video Tape, Hapco Co., Abingdon, VA, January 1996.

15. Kaufmann, E. J., Johns, K. W., Dexter, R. J., <u>Fractographic Examination of Failed Luminaire Components</u>, ATLSS Engineering Research Center, Lehigh University, Bethlehem, PA, 1997.

Appendix A – Fatigue Design Example

1. General

The following appendix details selected, necessary calculations that need to be performed on luminaire support structures in order to evaluated their fatigue strength.

1.1 Description

The structure in this appendix is the one that failed on Route 147 in southern New Jersey. The sign was checked for fatigue sensitive details based on the loads recommended in this report and Section 1.9.6 of the AASHTO Specifications. Because the structure is on a major highway, the importance factor is 1 in all calculations (Table 1.9.6.1 AASHTO). All calculations are performed in SI units.

1.2 Dimensions

The following dimensions represent the dimensions for the straight luminaire support structures that failed along Route 147.
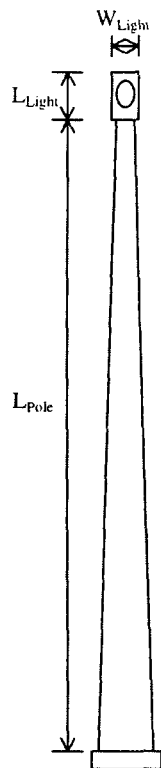
Light width = W_{Light} = 0.3048 m
Light length = L_{Light} = 0.7366 m
Pole length = L_{Pole} = 12.6492 m
Diameter of pole top = D_{Top} = 0.1524 m
Diameter of pole bottom = D_{Bottom} = 0.2032 m

59

2. Calculations of Limit State Fatigue Loads

This section illustrates the application of the two wind loading phenomena that are applicable to a luminaire support structures, i.e. natural wind gusts and vortex shedding.

2.1 Vortex Shedding

The support structure is checked using the design procedures for vortex shedding described in Chapter 4 of this report.

A dynamic finite element analysis (FEA) was performed to determine the relevant mode shapes and natural frequencies. As was described in Chapter 2 the mode shapes come in pairs for a perfectly symmetric structure in a three dimensional analysis, therefore only every other mode number is mentioned.

2.1.1 Mode One

From FEA the first mode natural frequency is 0.85 cycles/s. Calculate the critical wind velocity, V_{cr}, of the mode using Equation 4-2.
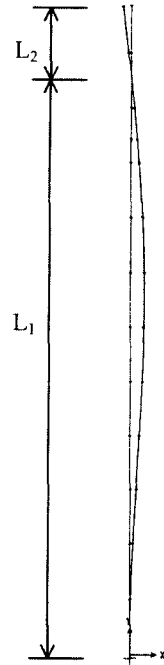
$$V_{cr} = \frac{f_n D}{S} = \frac{(0.85 cycles / s)(0.1778m)}{0.18} = 0.84 m / s$$

where f_n is the natural frequency, D is the average pole diameter, and S is the Strouhal number.

V_{cr} is not between 5 and 15 m/s therefore, this is not a valid mode shape for vortex shedding.

2.1.2 Mode Three

The third mode shape was determined from FEA and is displayed here.

$L_1 = 11.6586$ m
$L_2 = 0.9906$ m
$D_{Top} = 0.1524$ m
$D_{Bottom} = 0.2032$ m

From FEA the third mode natural frequency is 5.24 cycles/s. Calculate the critical wind velocity, V_{cr}, of the mode using Equation 4-2.

$$V_{cr} = \frac{f_n D}{S} = \frac{(5.24 cycles/s)(0.1778m)}{0.18} = 5.2m/s$$

where f_n is the natural frequency, D is the average pole diameter, and S is the Strouhal number.

V_{cr} is between 5 and 15 m/s therefore, this is a valid mode shape for vortex shedding.

Calculate the pressure from vortex shedding, P_{vs} for this mode shape using Equation 4-3.

$$P_{vs} = \frac{0.613(V_{cr}^2)C_d I_F}{2\zeta} = \frac{(0.613)(5.2m/s)^2(1.1)}{2(.01)} = 912Pa$$

61

where V_{cr} (m/s) is the critical wind velocity, C_d is the appropriate drag coefficient from Table 1.2.5C of the AASHTO Code, I_F is the Importance factor based on the location of the structure, and ζ is the damping ratio taken as 0.01 from experimental data.

Use the average diameter between inflection points to calculate the tributary areas to apply the pressure to.

$$A_1 = L_1 D_1 = (11.6586 \text{ m})(0.1778 \text{ m}) = 2.0729 \text{ m}^2$$

$$A_2 = L_2 D_2 = (0.9906 \text{ m})(0.1524 \text{ m}) = 0.1510 \text{ m}^2$$

where A_1 and A_2 are the tributary areas associated with L_1 and L_2 respectively, and D_1 and D_2 are the average diameters of sections L_1 and L_2 respectively.

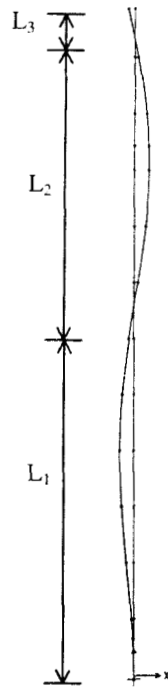The force per tributary area is calculated by:

$$(F_{vs})_1 = P_{vs} A_1 = (912 \text{ Pa})(2.0729 \text{ m}^2) = 1890 \text{ N}$$

$$(F_{vs})_2 = P_{vs} A_2 = (912 \text{ Pa})(0.1510 \text{ m}^2) = 138 \text{ N}$$

where $(F_{vs})_1$ and $(F_{vs})_2$ are the forces to be applied to sections L_1 and L_2 respectively.

2.1.2 Mode Five

The fifth mode shape was determined from FEA and is displayed here.

$L_1 = 6.9342$ m
$L_2 = 5.2578$ m
$L_3 = 0.4572$ m
$D_{Top} = 0.1524$ m
$D_{Bottom} = 0.2032$ m

From FEA the fifth mode natural frequency is 15.2 cycles/s. Calculate the critical wind velocity, V_{cr}, of the mode using Equation 4-2.

$$V_{cr} = \frac{f_n D}{S} = \frac{(15.2 cycles/s)(0.1778m)}{0.18} = 15.0 m/s$$

where f_n is the natural frequency, D is the average pole diameter, and S is the Strouhal number.

V_{cr} is between 5 and 15 m/s therefore, this is a valid mode shape for vortex shedding.

Calculate the pressure from vortex shedding, P_{vs} for this mode shape using Equation 4-3.

$$P_{vs} = \frac{0.613(V_{cr}^2)C_d I_F}{2\zeta} = \frac{(0.613)(15.0m/s)^2(1.1)}{2(.01)} = 7586 Pa$$

63

where V_{cr} (m/s) is the critical wind velocity, C_d is the appropriate drag coefficient from Table 1.2.5C of the AASHTO Code, I_F is the Importance factor based on the location of the structure, and ζ is the damping ratio taken as 0.01 from experimental data.

Use the average diameter between inflection points to calculate the tributary areas to apply the pressure to.

$$A_1 = L_1 D_1 = (6.9342 \text{ m})(0.1905 \text{ m}) = 1.321 \text{ m}^2$$

$$A_2 = L_2 D_2 = (5.2578 \text{ m})(0.1651 \text{ m}) = 0.8681 \text{ m}^2$$

$$A_3 = L_3 D_3 = (0.4572 \text{ m})(0.1524 \text{ m}) = 0.0697 \text{ m}^2$$

where A_1, A_2 and A_3 are the tributary areas associated with L_1, L_2 and L_3 respectively, and D_1, D_2 and D_3 are the average diameters of sections L_1, L_2 and L_3 respectively.

The force per tributary area is calculated by:

$$(F_{vs})_1 = P_{vs}A_1 = (7586 \text{ Pa})(1.321 \text{ m}^2) = 10021 \text{ N}$$

$$(F_{vs})_2 = P_{vs}A_2 = (7586 \text{ Pa})(0.8681 \text{ m}^2) = 6585 \text{ N}$$

$$(F_{vs})_3 = P_{vs}A_3 = (7586 \text{ Pa})(0.0697 \text{ m}^2) = 529 \text{ N}$$

where $(F_{vs})_1$, $(F_{vs})_2$ and $(F_{vs})_3$ are the forces to be applied to sections L_1, L_2 and L_3 respectively.

2.1.1 Mode Seven

From FEA the seventh mode natural frequency is 29.9 cycles/s. Calculate the critical wind velocity, V_{cr}, of the mode using Equation 4-2.

$$V_{cr} = \frac{f_n D}{S} = \frac{(29.9 cycles/s)(0.1778m)}{0.18} = 29.5 m/s$$

where f_n is the natural frequency, D is the average pole diameter, and S is the Strouhal number.

V_{cr} is not between 5 and 15 m/s therefore, this is not a valid mode shape for vortex shedding.

2.2 Natural Wind Gusts

It is assumed that the annual mean wind velocity is 5 m/s at the location of the failed luminaires. The luminaire is checked using the equivalent static pressure range of 250 Pa times the drag coefficient for natural wind gusts

$$P_{NW} = 250C_dI_F$$

where C_d is the appropriate drag coefficient from table 1.2.5C of the AASHTO Specification. The pressures due to natural wind gusts on the pole and light fixture are calculated by:

$$(P_{NW})_{Pole} = (250)(1.1)(1.0) = 275 \text{ Pa}$$

where 1.1 is the appropriate C_d for this geometry of pole.

$$(P_{NW})_{Light} = (250)(1.2)(1.0) = 300 \text{ Pa}$$

where 1.2 is the appropriate C_d for this geometry of luminaire.

The areas of the different components of the structure are calculated by:

$$A_{Pole} = L_{Pole}D_{Pole} = (12.6492 \text{ m})(0.1778 \text{ m}) = 2.2490 \text{ m}^2$$

$$A_{light} = L_{Light}W_{Light} = (0.7366 \text{ m})(0.3048 \text{ m}) = 0.2245 \text{ m}^2$$

The equivalent static load range applied to the sign is calculated by:

$$(F_{NW})_{Pole} = (P_{NW})_{Pole}A_{Pole} = (275 \text{ Pa})(2.2490 \text{ m}^2) = 619 \text{ N}$$

$$(F_{NW})_{Light} = (P_{NW})_{Light}A_{Light} = (300 \text{ Pa})(0.2245 \text{ m}^2) = 67 \text{ N}$$

3. Bending Moment Calculations

The moment at the shoe base-to-pole connection is calculated in this section.

3.1 Vortex Shedding

The moment at the shoe base-to-pole connection due to vortex shedding is calculated for each of the mode shapes in this section.

3.1.1 Mode Three

$$M_{vs} = (F_{vs})_1 \frac{L_1}{2} - (F_{vs})_2 (L_1 + \frac{L_2}{2}) =$$

$$1890N \left(\frac{11.6586m}{2} \right) - 138N \left(11.6586m + \frac{0.9906m}{2} \right) = 9340Nm$$

3.1.2 Mode Five

$$M_{vs} = (F_{vs})_1 \frac{L_1}{2} - (F_{vs})_2 (L_1 + \frac{L_2}{2}) + (F_{vs})_3 (L_1 + L_2 + \frac{L_3}{2}) =$$

$$10021N \left(\frac{6.9342m}{2} \right) - 6585N \left(6.9342m + \frac{5.2578m}{2} \right) + 529N \left(6.9342m + 5.2578m + \frac{0.4572m}{2} \right)$$

$$= 21660Nm$$

3.2 Natural Wind Gusts

The moment at the shoe base-to-pole connection due to natural wind gusts is calculated for each of the mode shapes in this section.

$$M_{NW} = (F_{NW})_{Pole} \frac{L_{Pole}}{2} + (F_{NW})_{Light} (L_{Pole} + \frac{L_{Light}}{2}) =$$

$$619N \left(\frac{12.6492m}{2} \right) + 67N \left(12.6492m + \frac{0.7366m}{2} \right) = 4790Nm$$

4. Stress Range Calculations

The stress range at the shoe base-to-pole connection for the controlling bending moment is calculated in this section.

4.1.1 Moment of Inertia

The moment of inertia of the pole at the shoe base-to-pole connection is calculated by:

$$I_{Pole} = \frac{\pi}{64}\left[D_{Pole}^{\;4} - (D_{Pole} - 2t_{Pole})^4\right] =$$

$$\frac{\pi}{64}\left[(0.2032m)^4 - (0.2032m - 2*0.0064m)^4\right] = 1.918\times10^{-5}m^4$$

4.1.2 Stress Range at Pole to Shoe Base Connection

Based on the calculations in section 3 vortex shedding in the fifth mode controls the shoe base-to-pole connection. The stress range at the shoe base-to-pole connection was calculated by:

$$(S_R)_{Pole-SB} = \frac{(M_{vs})c}{I_{Pole}} = \frac{(21660Nm)(0.1016m)}{1.918\times10^{-5}m^4} = 115MPa$$

The shoe base-to-pole connection is a category E detail. The corresponding CAFL is 13 MPa. Since the calculated stress range (115 MPa) was greater than the CAFL (13 MPa) the shoe base-to-pole connection was inadequately designed for fatigue.

67